ARTICLE

Activated PI3Kδ breaches multiple B cell tolerance checkpoints and causes autoantibody production

Anthony Lau[1,2], Danielle T. Avery[1], Katherine Jackson[1], Helen Lenthall[1], Stefano Volpi[3], Henry Brigden[1], Amanda J. Russell[1], Julia Bier[1,2], Joanne H. Reed[1,2], Joanne M. Smart[4], Theresa Cole[4], Sharon Choo[4], Paul E. Gray[5,6], Lucinda J. Berglund[6,7,8], Peter Hsu[6,9], Melanie Wong[6,9], Michael O'Sullivan[6,10], Kaan Boztug[11,12,13,14], Isabelle Meyts[15], Gulbu Uzel[16], Luigi D. Notarangelo[16], Robert Brink[1,2,6], Christopher C. Goodnow[1,6,17], Stuart G. Tangye[1,2,6]*, and Elissa K. Deenick[1,6,18]*

Antibody-mediated autoimmune diseases are a major health burden. However, our understanding of how self-reactive B cells escape self-tolerance checkpoints to secrete pathogenic autoantibodies remains incomplete. Here, we demonstrate that patients with monogenic immune dysregulation caused by gain-of-function mutations in *PIK3CD*, encoding the p110δ catalytic subunit of phosphoinositide 3-kinase (PI3K), have highly penetrant secretion of autoreactive IgM antibodies. In mice with the corresponding heterozygous *Pik3cd* activating mutation, self-reactive B cells exhibit a cell-autonomous subversion of their response to self-antigen: instead of becoming tolerized and repressed from secreting autoantibody, *Pik3cd* gain-of-function B cells are activated by self-antigen to form plasmablasts that secrete high titers of germline-encoded IgM autoantibody and hypermutating germinal center B cells. However, within the germinal center, peripheral tolerance was still enforced, and there was selection against B cells with high affinity for self-antigen. These data show that the strength of PI3K signaling is a key regulator of pregerminal center B cell self-tolerance and thus represents a druggable pathway to treat antibody-mediated autoimmunity.

Introduction

During B cell development in the bone marrow (BM), random recombination of genetic elements encoding the B cell antigen receptor (BCR) leads to the generation of a large number of self-reactive B cells (Wardemann et al., 2003). Multiple tolerance checkpoints exist in the BM and periphery to prevent these self-reactive B cells from becoming activated and producing patho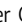genic autoantibodies. Thus, during development immature self-reactive B cells that encounter self-antigens can be censored in the BM through receptor editing or clonal deletion (Nemazee, 2017). If B cells escape these central tolerance mechanisms, they can become functionally silenced or anergized in the periphery to prevent them from forming antibody-secreting plasma cells or germinal centers (GCs) in response to self-antigen (Goodnow et al., 2005; Nemazee, 2017). However, if these anergized self-reactive B cells encounter foreign microbial antigens that cross-react with their BCR and concomitantly receive TLR costimulatory signals and T cell help, they can become activated to form GCs (Shlomchik, 2008). However, tolerance mechanisms also exist in the GC to ensure that self-reactive cells, either recruited into the GC because of cross-reactivity with foreign antigens or randomly generated through somatic hypermutation (SHM), are purged from the response, thereby preventing the secretion of high-affinity autoantibodies (Brink and Phan, 2018).

[1]Immunity and Inflammatory Diseases, Garvan Institute of Medical Research, Darlinghurst, New South Wales, Australia; [2]St. Vincent's Clinical School, Faculty of Medicine, UNSW Sydney, Sydney, Australia; [3]Clinica Pediatrica e Reumatologia, Centro per le malattie Autoinfiammatorie e Immunodeficienze, Istituto di Ricovero e Cura a Carattere Scientifico (IRCCS) Istituto Giannina Gaslini and Dipartimento di Neuroscienze, riabilitazione, oftalmologia, genetica e scienze materno-infantili (DINOGMI), Università degli Studi di Genova, Genova, Italy; [4]Department of Allergy and Immunology, Royal Children's Hospital Melbourne, Victoria, Australia; [5]School of Women's and Children's Health, UNSW Sydney, Sydney, Australia; [6]Clinical Immunogenomics Research Consortium of Australasia, Sydney, Australia; [7]Immunopathology Department, Westmead Hospital, Westmead, New South Wales, Australia; [8]Faculty of Medicine, University of Sydney, Sydney, New South Wales, Australia; [9]Children's Hospital at Westmead, New South Wales, Australia; [10]Department of Immunology and Allergy, Princess Margaret Hospital, Subiaco, Western Australia, Australia; [11]Ludwig Boltzmann Institute for Rare and Undiagnosed Diseases, Vienna, Austria; [12]CeMM Research Center for Molecular Medicine of the Austrian Academy of Sciences, Vienna, Austria; [13]St. Anna Children's Hospital, Department of Pediatrics and Adolescent Medicine, Medical University of Vienna, Vienna, Austria; [14]St. Anna Children's Cancer Research Institute (CCRI), Vienna, Austria; [15]Department of Immunology and Microbiology, Inborn Errors of Immunity, Department of Pediatrics, University Hospitals Leuven and KU Leuven, Leuven, Belgium; [16]Laboratory of Clinical Immunology and Microbiology, National Institute of Allergy and Infectious Diseases, National Institutes of Health, Bethesda, MD; [17]UNSW Cellular Genomics Futures Institute, UNSW Sydney, Sydney, Australia; [18]Faculty of Medicine, UNSW Sydney, Sydney, Australia.

*S.G. Tangye and E.K. Deenick contributed equally to this paper; Correspondence to Elissa K. Deenick: e.deenick@garvan.org.au.

1

The high frequency of antibody-mediated autoimmune disease in humans (Hayter and Cook, 2012) demonstrates that these processes are often dysregulated. However, it is still not clear exactly how these self-tolerance checkpoints are normally maintained and how they break down to precipitate autoimmunity. For example, what are the critical signaling pathways that distinguish recognition of self-antigens from foreign antigens? Further, how do these different signaling pathways trigger the inhibitory checkpoints needed to maintain self-tolerance, versus the B cell proliferation, GC formation, affinity maturation, and differentiation into antibody-secreting plasma cells that are necessary for host defense?

Recently, patients with a monogenic immune dysregulation condition caused by germline heterozygous, gain-of-function (GOF) mutations in *PIK3CD*, which encodes the p110δ catalytic subunit of phosphoinositide 3-kinase (PI3K), have been identified (Angulo et al., 2013; Coulter et al., 2017; Lucas et al., 2014). This has been termed activated PI3Kδ syndrome. PI3Ks are lipid kinases that play numerous important roles in cell growth, function, and survival. There are multiple classes of PI3Ks (class IA, IB, II, and III); however, the class IA PI3Ks, which include p110δ, are particularly important in immune signaling, where they are activated downstream of several receptors including the BCR, T cell receptor, CD19, and TLRs (Okkenhaug, 2013). Class IA PI3Ks are comprised of a p110 catalytic subunit (p110α, p110β, or p110δ), linked to a regulatory subunit (p85, p55, or p50). The p110α and p110β catalytic subunits are ubiquitously expressed, whereas p110δ is highly expressed in leukocytes. Class IA PI3Ks phosphorylate phosphatidylinositol-4,5-bisphosphate to generate phosphatidylinositol-3,4,5-trisphosphate, which acts as a second messenger molecule to further transduce signals to downstream molecules such as Akt and mTOR.

Patients with *PIK3CD* GOF mutations present with several clinical manifestations, including recurrent respiratory tract infections, hyper IgM, susceptibility to infection with herpes family viruses, bronchiectasis, hepatosplenomegaly, and increased rates of lymphoma (Coulter et al., 2017; Lucas et al., 2014; Maccari et al., 2018). Interestingly, ~40% of *PIK3CD* GOF patients also develop clinically relevant autoimmune disease, including autoimmune cytopenias, glomerulonephritis, and autoimmune thyroiditis (Coulter et al., 2017; Lucas et al., 2014; Maccari et al., 2018). Several recent studies have explored the pathogenesis of the immunodeficiency in these patients (Avery et al., 2018; Bier et al., 2019; Cannons et al., 2018; Cura Daball et al., 2018; Edwards et al., 2019; Preite et al., 2018; Preite et al., 2019; Ruiz-García et al., 2018; Stark et al., 2018; Wentink et al., 2017; Wentink et al., 2018; Wray-Dutra et al., 2018). These studies have revealed defects in B cells and CD4+ T cells, thereby elucidating mechanisms for poor antibody responses and susceptibility to respiratory infections, and altered natural killer and CD8+ T cell function, which provide an explanation for the viral susceptibility and possibly malignancy. However, far less is known about how these mutations cause autoimmunity.

To investigate this, we examined both patients with *PIK3CD* GOF mutations and a novel mouse model that carries an analogous pathogenic *Pik3cd* GOF mutation. Our analyses revealed a B cell–specific break in self-tolerance at the pre-GC stage with production of germline autoreactive IgM antibodies. In contrast, PI3K overactivation did not affect tolerance within the GC, establishing that distinct signaling pathways operate at different stages of antigen-induced B cell activation to ensure that tolerance is maintained.

Results

Patients with GOF mutations in *PIK3CD* have high levels of IgM autoantibodies

We first analyzed sera from *PIK3CD* GOF patients by autoantibody array. This revealed high levels of self-reactive IgM antibodies against diverse self-antigens, including those commonly seen in patients with systemic lupus erythematosus (SLE; Fig. 1 A and Fig. S1 A). In contrast, while there appeared to be IgG antibodies in patient sera that bound to some self-antigens, none of these IgG autoantibodies were found to be significantly different from those in healthy donors (Fig. S1 B), consistent with reduced isotype switching and decreased serum IgG levels in these patients (Angulo et al., 2013; Avery et al., 2018; Coulter et al., 2017; Lucas et al., 2014).

To more precisely track the breakdown of tolerance in these patients and the B cells that produce it, we focused on antibodies that used the *IGHV4-34* variable element. Use of this Ig variable element confers potentially pathogenic binding of the resulting secreted antibodies to N-linked N-acetyllactosamine determinants expressed by the I/i blood group antigens on erythrocytes, as well as other cell surface glycoproteins such as CD45R/B220 on B cells (Cappione et al., 2004).

To measure the relative levels of self-reactive serum VH4-34 antibodies, we incubated B cells from healthy donors with control or *PIK3CD* GOF patient serum and detected VH4-34–containing antibody bound to the surface using the anti-idiotype monoclonal antibody 9G4, which binds VH4-34 (Potter et al., 1993). Compared with serum from healthy donors, serum from *PIK3CD* GOF patients resulted in 10 times higher staining with 9G4 on normal transitional B cells (Fig. 1, B and C). A similar pattern was observed for binding to normal naive and memory B cells, although the intensity of staining was reduced (data not shown), consistent with lower levels of the CD45R/B220 isoform recognized by the VH4-34 antibody on memory B cells (Bleesing and Fleisher, 2003; Cappione et al., 2004). Since ~60% of the *PIK3CD* GOF patients in our cohort had clinically defined autoimmune manifestations at the time of serum collection, these results reveal a much more highly penetrant failure of self-tolerance to ubiquitous autoantigens in patients with germline *PIK3CD* GOF mutations than previously appreciated.

Patients with *PIK3CD* GOF mutations have increased frequencies of B cells that use the autoreactive IGHV4-34 variable region

In the B cell repertoire of healthy donors, ~5–10% of newly formed B cells display IgM antibodies on their surface that use the *IGHV4-34* variable element (Pugh-Bernard et al., 2001). These VH4-34+ B cells, however, are restrained by tolerance
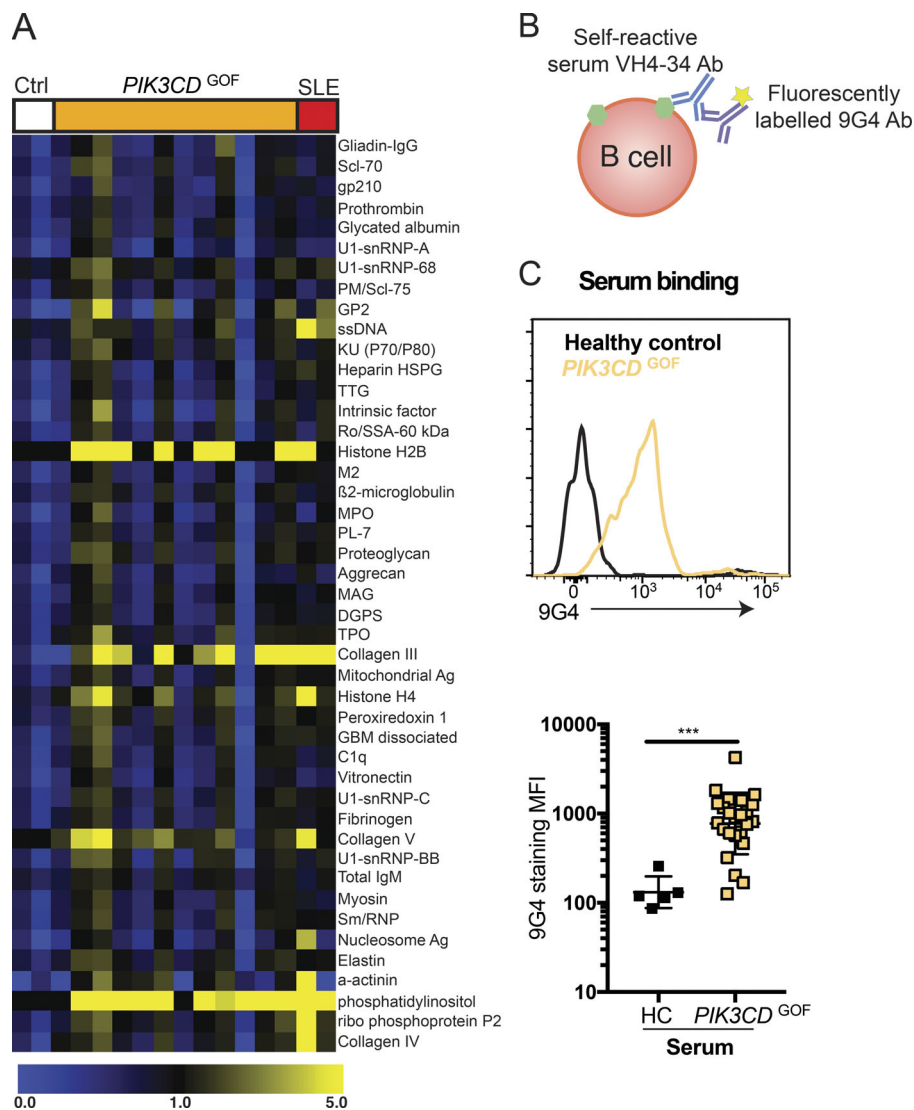
Lau et al.
Activated PI3Kδ breaks B cell tolerance

Journal of Experimental Medicine
https://doi.org/10.1084/jem.20191336

2

Figure 1. **PIK3CD GOF patients have autoreactive serum antibodies. (A)** Heatmap showing relative binding of serum IgM from healthy controls (Ctrl; $n = 2$), PIK3CD GOF ($n = 12$), or SLE ($n = 2$) patients to different self-antigens. Shown are antibodies with statistical difference as detected by significance analysis of microarray test. ssDNA, single-stranded DNA. **(B and C)** Measurement of serum VH4-34 autoantibodies against I/i blood group carbohydrates on the surface of transitional B cells. Serum from PIK3CD GOF patients or healthy controls was incubated with peripheral blood mononuclear cells from healthy controls (HC), and serum VH4-34 antibodies that bound to transitional B cells were then detected with the 9G4 anti-idiotypic monoclonal antibody, which binds unmutated VH4-34. Each point represents an individual patient ($n = 5$) or healthy control ($n = 24$) combined from four separate experiments; line gives geometric mean and SD. Significant differences were determined by Mann-Whitney test. ***, $P < 0.001$. See also Fig. S1.

mechanisms and thus persist as desensitized or anergic cells in the periphery (Goodnow et al., 2005; Nemazee, 2017; Pugh-Bernard et al., 2001). To determine if the increased serum VH4-34 antibodies were associated with alterations in the proportions of B cells expressing VH4-34 BCRs, we stained B cells from healthy donors or PIK3CD GOF patients with the 9G4 anti-idiotype antibody that recognizes VH4-34 and quantified expression levels by flow cytometry (Fig. 2 A). In the patients we observed a shift in 9G4 staining for the entire B cell population, likely representing painting of B cells with serum VH4-34 antibodies, while the very brightly stained population is likely B cells expressing endogenous VH4-34 BCR (Fig. 2 A). PIK3CD GOF patients had an increased percentage of these VH4-34[Hi] B cells in all subsets (transitional, naive, and memory; Fig. 2 B), suggesting they had increased proportions of autoreactive B cells.

To confirm this and assess the immunoglobulin repertoire at the global level, we sorted transitional or naive B cells from healthy donors and PIK3CD GOF patients and performed deep sequencing of the IgM transcripts (Fig. 2 C and Fig. S2). The repertoires of transitional and naive B cells for PIK3CD GOF

patients showed the use of diverse IGHV gene segments (Fig. S2). However, consistent with our FACS staining (Fig. 2 B), there was an over-representation of BCRs using IGHV4-34 in the patients compared with healthy donors for both the transitional and naive compartments (Fig. 2 C and Fig. S2). This increased IGHV4-34 utilization was accompanied by a decrease in the usage of IGHV3-23, the most frequently rearranged IGHV gene segment in healthy donors, in patients (Fig. S2). Thus, patients with mutations that cause increased PI3K signaling displayed an increase in B cells expressing autoreactive receptors and in serum autoantibodies.

Development of self-reactive Pik3cd GOF B cells in the BM

To establish the basis for this failed self-tolerance in humans with activated PI3K, we used a CRISPR/Cas9-generated mouse line (Avery et al., 2018) carrying the murine equivalent (E1020K) of the most common human PIK3CD GOF mutation (E1021K; Coulter et al., 2017), and crossed it with SW[HEL] BCR knock-in mice expressing the HyHEL10 BCR that recognizes hen-egg lysozyme (HEL; Phan et al., 2003). We then generated BM chimeras in which these SW[HEL] B cells developed in the
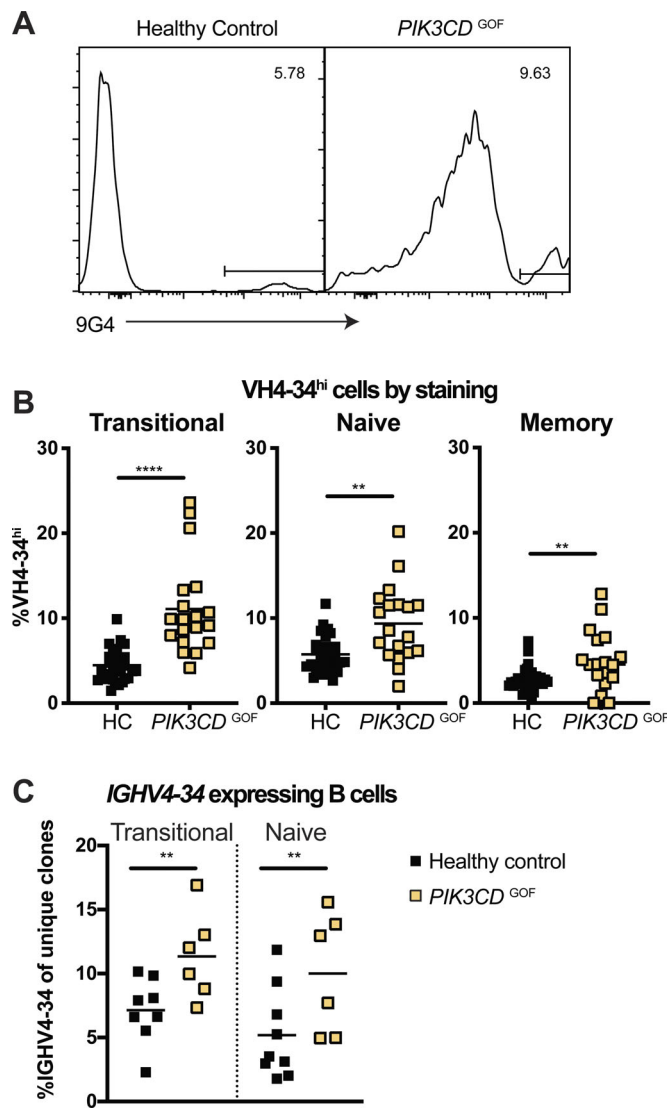
Figure 2. **B cells expressing autoreactive BCRs are increased in *PIK3CD* GOF patients. (A and B)** B cells from healthy controls or *PIK3CD* GOF patients were stained with the anti-idiotypic antibody 9G4, which binds the VH4-34 heavy chain. The general increase in 9G4 staining on B cells likely represents binding of serum VH4-34 antibodies to B cells, while the very brightly staining population corresponds to B cells endogenously expressing surface VH4-34 antibodies. **(A)** Representative staining on total B cells is shown. **(B)** Percentage of VH4-34^{hi} cells in each B cell population, as determined by flow cytometry. Each point represents an individual healthy control (HC; $n = 31$) or patient ($n = 18–19$). **(C)** mRNA was prepared from sorted transitional or naive B cell populations, and *IGHM* cDNA was amplified, deep-sequenced, and analyzed to calculate the percentage of unique clones that used the *IGHV4-34* element. Each point represents an individual healthy control ($n = 8–9$) or patient ($n = 6$); line shows mean. Significant differences were determined by Mann-Whitney (B) or ANOVA Tukey (C) test. ****, P < 0.0001; **, P < 0.01. See also Fig. S2.

presence of membrane-bound HEL[3X] (mHEL[3X], a mutant of HEL engineered to bind the HyHEL10 BCR with low affinity; Paus et al., 2006) expressed as a ubiquitous self-antigen (Burnett et al., 2018; Chan et al., 2012; Fig. 3 A).

In this system, the lower-affinity cell surface antigen does not provide a sufficiently strong signal to completely purge SW$_{HEL}$

cells from the developing B cell repertoire. Consequently, self-reactive WT SW$_{HEL}$ B cells reach the periphery (Burnett et al., 2018). Thus, equal numbers of WT SW$_{HEL}$ pre-pro-B, pro-B, pre-B, and immature B cells were observed irrespective of the presence of self-antigen (Fig. 3, B–D). In contrast, a significant reduction in the number of mature recirculating self-reactive WT SW$_{HEL}$ B cells was observed (Fig. 3, C and D). The stronger PI3K signaling in *Pik3cd*[GOF] SW$_{HEL}$ B cells resulted in slightly altered B cell development in the BM, with increased percentages of pro- and pre- and decreased immature *Pik3cd*[GOF] SW$_{HEL}$ B cells observed regardless of self-reactivity (Fig. 3, B–D). This is consistent with previous observations of increased pro- and pre-B cells in the endogenous repertoire of *Pik3cd*[GOF] mice, as well as of pre-B and immature B cells in the BM of patients with *PIK3CD* GOF mutations (Avery et al., 2018; Preite et al., 2018; Stark et al., 2018; Wray-Dutra et al., 2018). As with WT cells, we observed dramatically reduced proportions of mature self-reactive *Pik3cd*[GOF] SW$_{HEL}$ B cells (Fig. 3, B–D). Thus, increased PI3K signaling did not greatly alter the development of low-affinity self-reactive cells in the BM.

Pik3cd GOF self-reactive B cells escape peripheral tolerance and acquire a mature phenotype

Following development in the BM, WT low-affinity self-reactive SW$_{HEL}$ B cells migrate to the spleen as CD93^{+} transitional B cells, which then mature into short-lived anergic CD93^{−}IgM^{lo}IgD^{+} B cells (Fig. 4, A and B). As a consequence of this peripheral tolerance checkpoint, the number and frequency of autoreactive WT SW$_{HEL}$ B cells is decreased ~20-fold compared with non–self-reactive SW$_{HEL}$ cells that developed in the absence of mHEL[3X] self-antigen (Fig. 4, A and B; and Fig. S3).

Transitional self-reactive *Pik3cd*[GOF] SW$_{HEL}$ B cells were also decreased in numbers similar to WT self-reactive SW$_{HEL}$ cells (Fig. S3). However, self-reactive *Pik3cd*[GOF] SW$_{HEL}$ B cells exhibited a dramatic failure of peripheral tolerance at the mature stage, with a marked expansion of CD93^{−} B cells (Fig. 4, A and B; and Fig. S3). Most of the accumulating self-reactive *Pik3cd*[GOF] B cells had a marginal zone phenotype (MZ; CD23^{−}CD21^{+}CD1d^{+}IgD^{lo}; Fig. 4, C and D; and Fig. S3), in contrast to self-reactive WT B cells that are excluded from the MZ compartment.

Pik3cd GOF B cells have altered anergy induction

The accumulation of self-reactive MZ B cells suggested that anergy induction may be defective in *Pik3cd*[GOF] B cells. Thus, we examined expression of surface IgM, which is characteristically down-regulated on anergic B cells that have been chronically stimulated by self-antigen (Burnett et al., 2018; Goodnow et al., 1988; Goodnow et al., 2005; Nemazee, 2017). WT self-reactive SW$_{HEL}$ B cells down-regulated surface IgM expression more than fourfold (Fig. 5, A and B), as well as their total HEL-binding surface antibody (approximately threefold; Fig. S4), compared with non–self-reactive B cells. *Pik3cd*[GOF] self-reactive SW$_{HEL}$ B cells also down-regulated IgM expression on the transitional and follicular populations (Fig. 5, A and B). In contrast, self-reactive *Pik3cd*[GOF] SW$_{HEL}$ MZ B cells maintained surface IgM expression at high levels similar to non–self-reactive MZ B cells, despite their exposure to mHEL[3X] (Fig. 5, A and B), thereby revealing defective induction of anergy in these cells.
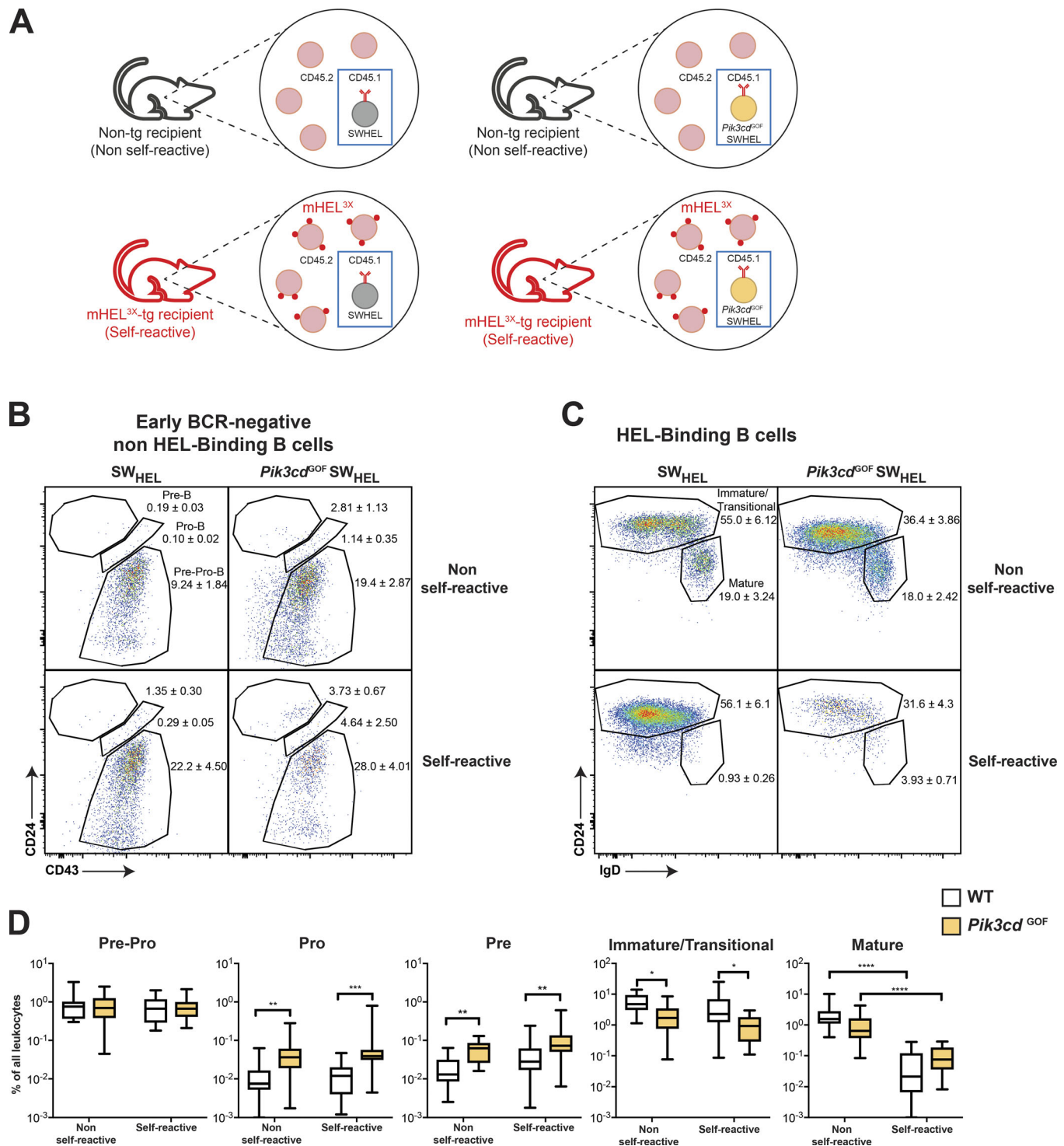
Figure 3. Development of self-reactive *Pik3cd* GOF B cells in the BM. (A) Four different types of BM chimeric mice were constructed by transplanting mixtures of CD45.1[+] RAG.SW$_{HEL}$ and CD45.2[+] nontransgenic (non-tg) BM into recipient mice that did or did not express membrane HEL[3X]. The CD45.1[+] RAG.SW$_{HEL}$ BM was either WT or *Pik3cd^{GOF}*, while the CD45.2[+] BM was WT for both *Rag1* and *Pik3cd*; thus, WT T and B cells with endogenous repertoires were derived from the CD45.2[+] BM. In chimeras where SW$_{HEL}$ cells are denoted as self-reactive, the recipients and all CD45.2^{+} blood cells expressed membrane HEL[3X], while control chimeras were identical except that they lacked the membrane HEL[3X] gene ("non self-reactive"). BM was harvested from chimeric mice 8–15 wk after reconstitution. SW$_{HEL}$ cells were identified as CD45.1[+]B220^{+} cells. **(B)** Plots show early BCR-negative cells stained with CD43 and CD24 to identify pre-pro-, pro-, and pre-B cells. Numbers are each population as a percentage of CD45.1[+]B220^{+} cells (mean ± SEM of all mice). **(C)** Plots show HEL-binding cells gated on CD24 and IgD to determine percentages of immature/transitional and mature B cell populations. Representative pseudocolor plots are shown for each condition. Numbers give each population as a percentage of CD45.1[+]B220^{+} cells (mean ± SEM of all mice). **(D)** Graphs show indicated populations as a percentage of total BM cells (the center line shows the median, box limits show the upper and lower quartiles, and whiskers show the minimum and maximum). All panels represent n = 17–21 mice per condition combined from nine experiments. Significant differences were determined using two-way ANOVA. *, $P < 0.05$; **, $P < 0.01$; ***, $P < 0.001$; ****, $P < 0.0001$.

Figure 4. Overactive PI3K breaks peripheral B cell tolerance, enabling expansion and persistence of self-reactive B cells. BM chimeras were generated as above; spleens were harvested and analyzed by flow cytometry 8–15 wk later. **(A)** R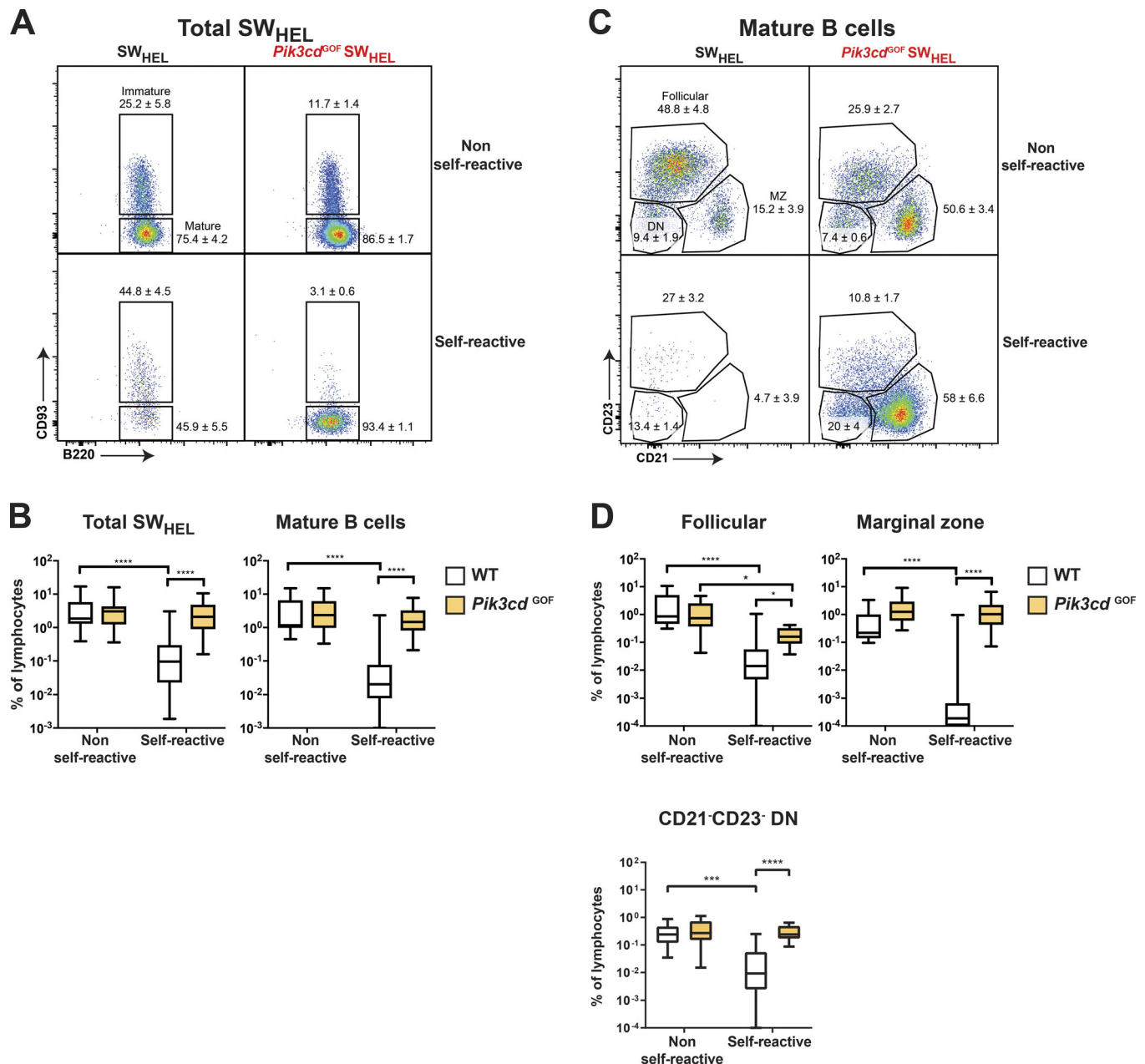epresentative plots of SW$_{HEL}$ B cells and of transitional (CD93$^+$) and mature (CD93$^-$) B cells. Numbers give each subset as a percentage of total B cells (mean ± SEM of all mice). **(B)** Graphs show percentages of total SW$_{HEL}$ and mature SW$_{HEL}$ cells among splenic lymphocytes. **(C)** Representative plots gated on mature SW$_{HEL}$ cells, showing the percentages (mean ± SEM of all mice) of follicular (CD23$^+$CD21^{med}) or MZ (CD23$^-$CD21^{high}) among total B cells. **(D)** Graphs show percentage of follicular and MZ SW$_{HEL}$ cells among all splenic lymphocytes. In B and D, the center line shows the median, box limits show the upper and lower quartiles, and whiskers show the minimum and maximum. All panels represent n = 11–20 mice per group combined from five to nine experiments. Significant differences were determined using two-way ANOVA. *, P < 0.05; ***, P < 0.001; ****, P < 0.0001. See also Fig. S3.

Another hallmark of B cell anergy is the failure to up-regulate CD86 upon binding to specific antigen by the BCR (Cooke et al., 1994; Eris et al., 1994). Accordingly, we tested the ability of self-reactive SW$_{HEL}$ cells to respond to HEL stimulation in vitro. While non–self-reactive WT and *Pik3cd*^{GOF} SW$_{HEL}$ cells up-regulated CD86 strongly in response to HEL, WT self-reactive SW$_{HEL}$ cells failed to do so (Fig. 5, C and D). In contrast, CD86 induction was not only intact in *Pik3cd*^{GOF} self-reactive SW$_{HEL}$

cells but was enhanced compared with non–self-reactive *Pik3cd*^{GOF} SW$_{HEL}$ cells (Fig. 5, C and D).

Self-reactive *Pik3cd* GOF B cells form spontaneous plasmablasts and GCs
Given the high levels of autoreactive IgM antibodies detected in *PIK3CD* GOF patients (Fig. 1 A), we next assessed the BM chimeras for the presence of anti-HEL antibodies and antibody-
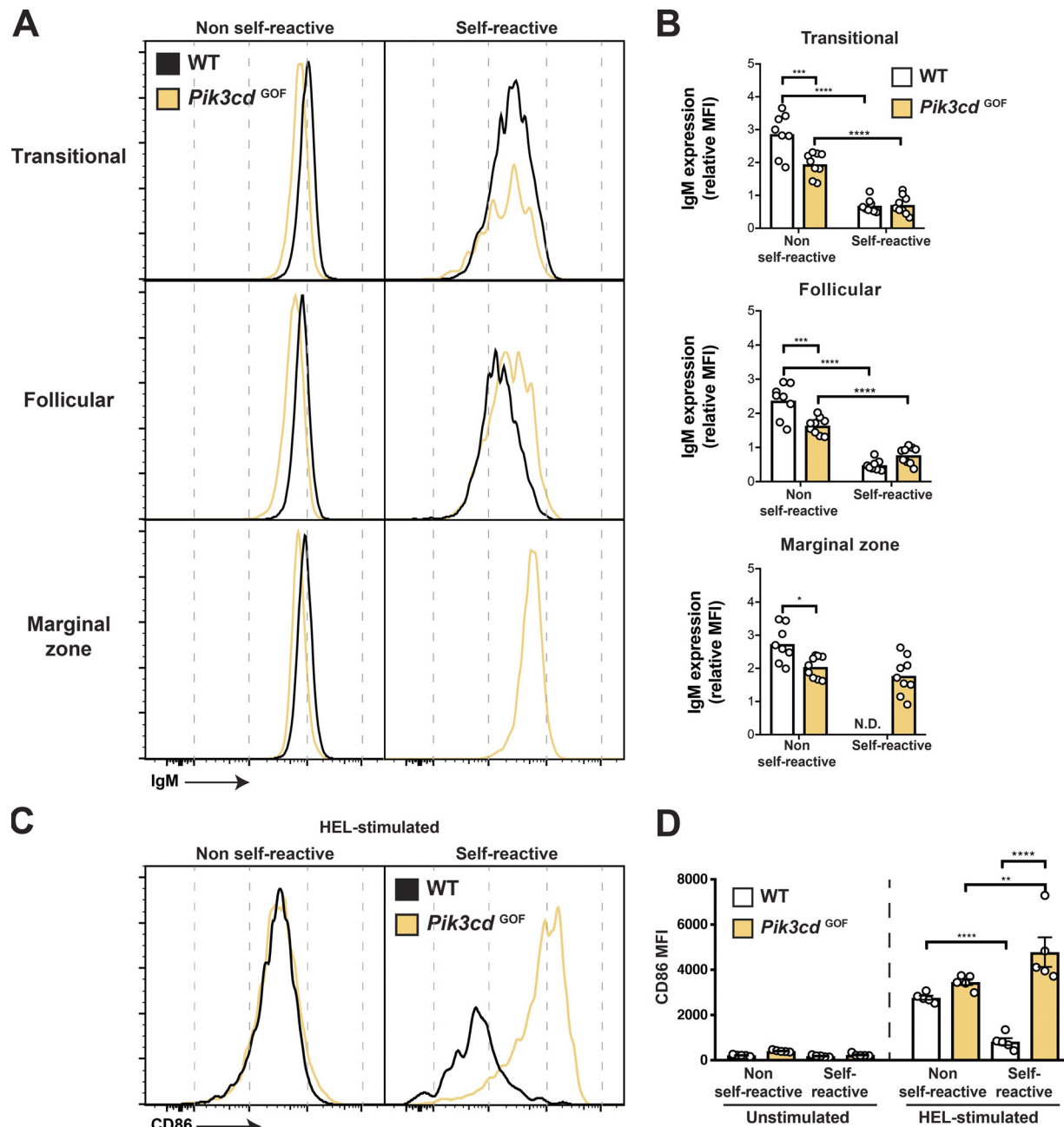
Figure 5. ***Pik3cd* GOF B cells show failed induction of anergy. (A)** Splenocytes from BM chimeras were assessed for expression of IgM on transitional, follicular, and MZ SW$_{HEL}$ cells. Representative histogram plots are shown. **(B)** Graphs show IgM MFI expressed relative to IgM expression on WT CD45.2$^+$ polyclonal follicular cells. Each point represents an individual mouse; bars show means (n = 8–9). N.D., not done, as insufficient numbers of MZ B cells were generated to be confidently analyzed. **(C and D)** Splenocytes from chimeric mice were either unstimulated or stimulated in vitro with HEL for 18 h; expression of CD86 was then determined by flow cytometry. Histograms show representative staining of CD86 on HEL-stimulated SW$_{HEL}$ cells (C), and the graph shows CD86 MFI of unstimulated or HEL-stimulated cells (D). Each point represents an individual mouse; bars show means ± SEM (n = 5 mice per group, combined from two experiments). Significant differences were determined using two-way ANOVA. *, P < 0.05; **, P < 0.01; ***, P < 0.001; ****, P < 0.0001. See also Fig. S4.

secreting cells. Importantly, as these chimeras were generated using SW$_{HEL}$ *Pik3cd*^{GOF} mice on a Rag1-deficient background, the only T cells present in these chimeras derive from the WT BM. Thus, any autoantibody production observed was independent of the effects of *Pik3cd* GOF CD4$^+$ T cells. Self-reactive *Pik3cd*^{GOF} SW$_{HEL}$ B cells not only evaded self-tolerance checkpoints to accumulate as IgM^{hi} antigen-responsive MZ B cells, but in the

absence of any immunization, they spontaneously formed IgM$^+$ plasmablasts (Fig. 6, A and B). Furthermore, these cells produced ~100 times more serum anti-HEL IgM than non–self-reactive *Pik3cd*^{GOF} SW$_{HEL}$ B cells, and almost 1,000 times more than self-reactive WT SW$_{HEL}$ B cells (Fig. 6 C). The absence of plasmablasts derived from *Pik3cd*^{GOF} cells in the non–self-reactive control chimeras indicates that this was self-antigen driven
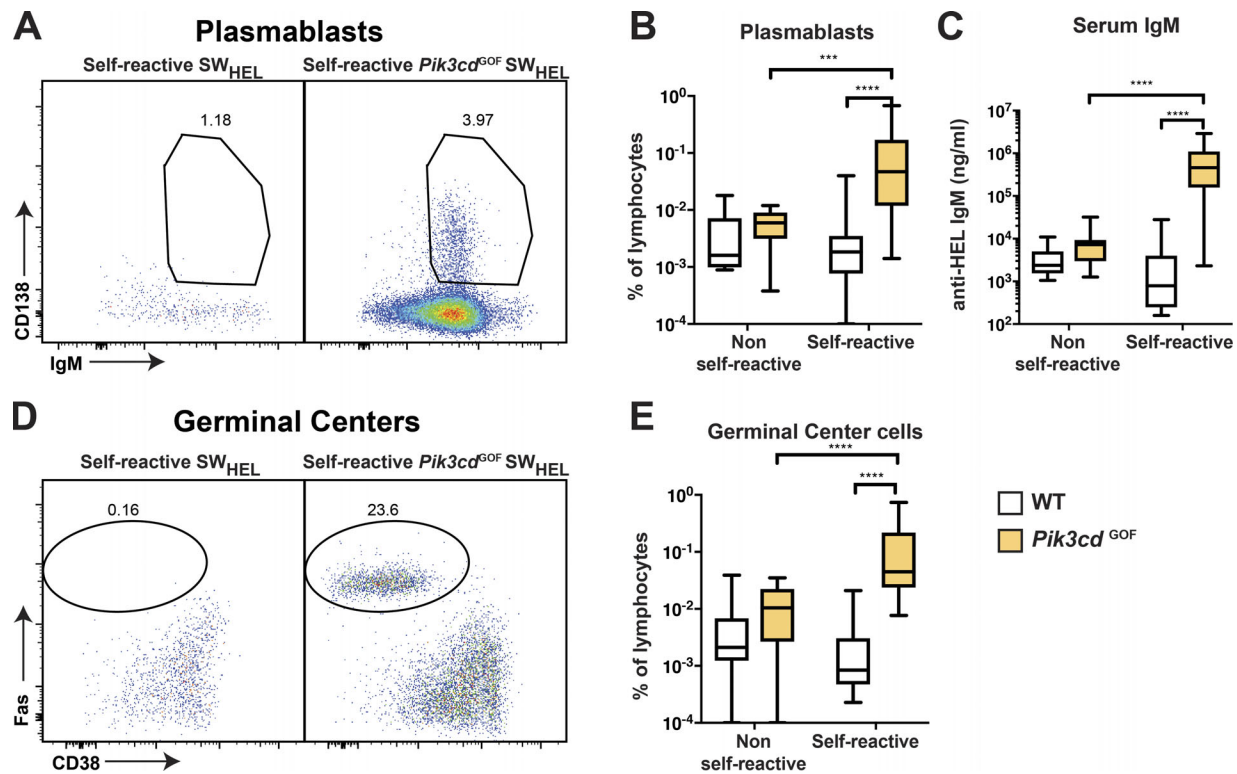
Figure 6. Self-reactive *Pik3cd* GOF B cells spontaneously generate plasmablasts secreting high levels of autoantibody and form GC B cells. BM chimeras were generated as above. **(A and B)** Spleens were stained to identify SW$_{HEL}$ IgM plasmablasts (IgM$^+$CD138^{hi}). **(C)** Levels of anti-HEL IgM in the serum of chimeric mice. **(D and E)** Spleens were stained to identify SW$_{HEL}$ GC B cells (Fas$^+$CD38^{lo}). The center line shows the median, box limits show the upper and lower quartiles, and whiskers show the minimum and maximum (n = 15–23 mice per group, combined from nine experiments). Significant differences were determined using two-way ANOVA. ***, P < 0.001; ****, P < 0.0001. See also Fig. S5.

and not the result of the *Pik3cd* GOF mutation per se (Fig. 6 B and Fig. S5). Thus, activated PI3K converted the tolerogen, mHEL^{3X}, into an immunogen that triggered plasmablast formation. Notably, self-antigen–induced autoantibody secretion was confined to the IgM isotype (Fig. 6 C and Fig. S5), consistent with the decreased ability of *Pik3cd*^{GOF} B cells to undergo class switch recombination (Avery et al., 2018; Preite et al., 2018; Wray-Dutra et al., 2018) and the paucity of IgG autoreactive antibodies in *PIK3CD* GOF patients (Fig. S1).

Enlarged GCs have been described in some patients with *PIK3CD* GOF (Crank et al., 2014; Lucas et al., 2014) as well as in mouse models of *Pik3cd*^{GOF} (Preite et al., 2018; Stark et al., 2018; Wray-Dutra et al., 2018). Therefore, we assessed whether *Pik3cd*^{GOF} B cells were induced to form GCs in response to self-antigen. Very few GC B cells were generated from WT or *Pik3cd*^{GOF} SW$_{HEL}$ non–self-reactive B cells or WT SW$_{HEL}$ self-reactive B cells. However, in stark contrast, self-reactive *Pik3cd*^{GOF} SW$_{HEL}$ B cells formed significant numbers of GC B cells (Fig. 6, D and E; and Fig. S5).

To demonstrate that this breach of tolerance is B cell intrinsic, and not a consequence of either overactive PI3K in other immune cells or masking of self-antigen by the high serum anti-HEL antibody levels present in the mice, we constructed mixed BM chimeras in which half of the developing self-reactive SW$_{HEL}$ B cells were *Pik3cd*^{GOF} and half were WT (Fig. S5 D). Under these circumstances, only the *Pik3cd*^{GOF} SW$_{HEL}$ B cells

accumulated as MZ B cells, plasmablasts, and GC cells, establishing that these defects are indeed B cell intrinsic (Fig. S5, E–G).

Self-reactive *Pik3cd* GOF plasmablasts express unmutated Ig V genes

We next tested if the self-antigen–driven formation of plasmablasts and GC cells from *Pik3cd*^{GOF} SW$_{HEL}$ B cells was accompanied by SHM, a process that normally occurs in the GC and can give rise to high-affinity B cells (Brink and Phan, 2018). Sequencing of the antibody heavy chain variable region from single sorted cells revealed that the GC B cell population had undergone considerable SHM (Fig. 7 A). In contrast, the plasmablast population lacked somatic mutations and continued to express germline-unmutated heavy chain variable region genes (Fig. 7 A). Thus, the autoreactive plasmablasts are likely derived from B cell activation outside of GCs.

Maintenance of self-tolerance in the GC is independent of activated PI3K

To determine the role of PI3K signaling in regulating self-tolerance in the GC, we assessed whether the somatic mutations acquired in the BCR of *Pik3cd*^{GOF} GC B cells increased their affinity for HEL^{3X}. Among the mutations present in the antibody heavy chain variable region of *Pik3cd*^{GOF} self-reactive GC B cells, there was a notable absence of the canonical Y53D mutation
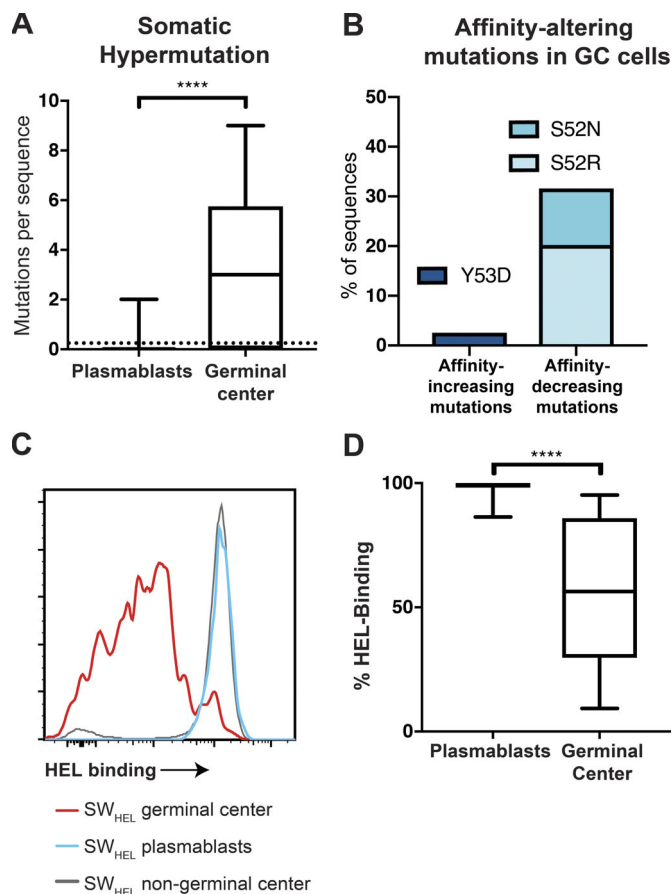
A
Somatic Hypermutation

B
Affinity-altering mutations in GC cells

C

- SW_HEL germinal center
- SW_HEL plasmablasts
- SW_HEL non-germinal center

D

Figure 7. ***Pik3cd* GOF antibody-secreting plasmablasts express unmutated antibody variable region genes.** Individual *Pik3cd*^GOF self-reactive plasmablasts (*n* = 25) and GC (*n* = 88) cells were sorted from nine different mice in six different experiments, and then the antibody heavy chain variable region of each cell was sequenced. **(A)** Graphs show the number of nucleotide mutations per cell, the center line shows the median, box limits show the upper and lower quartiles, and whiskers show the minimum and maximum. The dashed line shows the mean background rate of mutations detected in non-GC SW_HEL B cells. **(B)** Percentage of mutated GC sequences with the canonical affinity-increasing mutation at tyrosine (Y) 53 (Y53D) and the known affinity-decreasing mutations at position serine (S) 52 (S52N and S52R). **(C and D)** Cells were stained to identify the level of HEL binding by surface BCR. **(C)** Histograms show representative staining. **(D)** Graphs show the percentage of SW_HEL plasmablasts and GC cells that retained the ability to bind HEL (the center line shows the median, box limits show the upper and lower quartiles, and whiskers show the minimum and maximum (*n* = 15–19 mice combined from seven experiments). Significant differences were determined using Mann-Whitney test. ****, P < 0.0001.

(Fig. 7 B) that increases affinity for HEL^3X by 80-fold and is recurrently selected when HEL^3X is encountered as a foreign antigen (Phan et al., 2006). We have previously shown that *Pik3cd*^GOF SW_HEL cells acquire this Y53D affinity-enhancing mutation at normal rates when responding to immunization with HEL^2x conjugated to sheep RBC, indicating that *Pik3cd* GOF does not disrupt affinity maturation to foreign antigens (Avery et al., 2018). Thus, the lack of affinity maturation we observed here in *Pik3cd*^GOF SW_HEL GC B cells (Fig. 7 B) was specific to cells responding to self-antigen, rather than a generic defect in affinity maturation due to hyperactive PI3K signaling. Instead,

~30% of *Pik3cd*^GOF self-reactive GC B cells acquired mutations that dramatically reduce the affinity of the BCR for HEL^3X (S52N and S52R; Fig. 7 B; Burnett et al., 2018; Butt et al., 2015). Again, this contrasted markedly with the response of *Pik3cd*^GOF SW_HEL cells to foreign antigens, where only 10% of cells acquired mutations at S52 (Avery et al., 2018), of which <50% (that is <5% of total cells) were S52N or S52R mutations (data not shown). Consistent with this, a large proportion of GC B cells derived from *Pik3cd*^GOF SW_HEL B cells lost the ability to bind HEL (Fig. 7, C and D). Thus, although introduction of the *Pik3cd* GOF mutation results in B cell–intrinsic self-antigen–driven GC formation, once in the GC, there is strong negative selective pressure against high-affinity self-reactive B cells, as observed for normal GCs induced by foreign antigen (Burnett et al., 2018; Butt et al., 2015).

Discussion

Our parallel studies of humans and mice with germline *PIK3CD* GOF mutations identified a novel mechanism underlying B cell–mediated autoimmunity, where a normally tolerizing signal delivered by low-affinity membrane-bound self-antigens (e.g., I/i carbohydrate in patients or membrane HEL^3X in mice) to BCRs on self-reactive B cells is converted into a potent activating signal by aberrant PI3K p110δ signaling. Consequently, these B cells are induced to produce large amounts of serum IgM autoantibody against these antigens as well as form GCs.

To understand this further, we systematically dissected which tolerance checkpoints are controlled by PI3K signaling. We saw no evidence of altered development of *Pik3cd*^GOF B cells in the BM in response to the presence of self-antigen. Furthermore, there were similar decreases in immature self-reactive splenic B cells irrespective of whether they were WT or *Pik3cd* GOF. We did, however, see an increase in the percentage VH4-34^+ transitional B cells in patients, suggesting either that PI3K GOF may alter the deletion of these cells in the BM or enable increased survival or proliferation of autoreactive transitional cells in the periphery. Consistent with increased positive selection of autoreactive PI3K GOF B cells, there was a large expansion of autoreactive B cells at the mature cell stage in the spleens of *Pik3cd*^GOF mice. Further, self-reactive *Pik3cd*^GOF B cells bypassed the anergy checkpoint in mature B cells, evidenced by these cells undergoing spontaneous activation to form GCs and extrafollicular unmutated plasmablasts.

PI3K has previously been implicated in autoimmunity. Indeed, expression and/or function of PTEN or SHIP1, phosphatases that antagonize the PI3K pathway, are increased in anergic B cells (Browne et al., 2009; O'Neill et al., 2011; Smith et al., 2019). Similarly, expression of constitutively active p110α, deletion of PTEN or SHIP1, or overexpression of CD19, one of the B cell coreceptors that recruits and activates PI3K, all disrupt B cell tolerance (Akerlund et al., 2015; Browne et al., 2009; Greaves et al., 2019; Inaoki et al., 1997; Leung et al., 2013). However, the break in tolerance we observed here differs in multiple ways from these previous findings. First, while constitutively active p110α compromised central tolerance, it did not result in production of autoantibodies, suggesting either that

p110α and p110δ may play different roles in B cell tolerance, or that differences in signal strength alter these outcomes (Greaves et al., 2019). Second, while previous studies of PTEN or SHIP1 deficiency or CD19 overexpression in self-reactive B cells showed heightened production of IgM autoantibodies (Akerlund et al., 2015; Browne et al., 2009; Inaoki et al., 1997; Leung et al., 2013; Taylor et al., 2006), when the level of antibody production was directly compared in the presence and absence of the self-antigen, the level was the same, suggesting this was spontaneous antigen-independent antibody production (Browne et al., 2009; Inaoki et al., 1997; Setz et al., 2019). In contrast, we saw that antibody production was dramatically increased in the presence of the self-antigen (Fig. 6 C). Third, in PTEN and SHIP1 deficiency, defective anergy induction could, at least in part, be attributed to the presence of circulating autoantibody, which blocks availability of self-antigen able to induce anergy in self-reactive B cells and therefore was not intrinsic to developing self-reactive cells (Akerlund et al., 2015; Browne et al., 2009). This markedly contrasts our findings, which unequivocally established that the breach in self-tolerance was B cell intrinsic and limited to B cells carrying the $Pik3cd^{GOF}$ mutation. Lastly, these previous studies did not report formation of self-reactive GCs (Browne et al., 2009; Getahun et al., 2016; Taylor et al., 2006), whereas we saw abundant generation of spontaneous GCs from $Pik3cd^{GOF}$ B cells. It is not clear whether these differences reflect a particular effect of p110δ GOF that differs qualitatively and quantitatively from other signaling disruptions that amplify PI3K activation or whether this partially reflects the difference between the nature of the antigen used in the different studies: high-affinity soluble or membrane versus lower-affinity membrane-bound antigen. It is interesting to note that the autoantibodies identified in $PIK3CD$ GOF patients are largely against antigens that would be repetitive or membrane bound such as the I/I antigens, collagen, or histones. Thus, PI3K overactivation may render patients particularly susceptible to breaches in self-tolerance toward these types of high-avidity self-antigens.

In addition to the BCR, PI3K is activated downstream of many receptors that are important mediators of T cell help to B cells, such as CD40 and IL-21R (Ostiguy et al., 2007; Ren et al., 1994; Zeng et al., 2007), as well as microbe-sensing TLRs (Durand et al., 2009). Thus, while self-antigen usually only provides signal 1, hyperactive PI3K signaling may mimic these other signals that would normally occur only in B cells recognizing foreign microbes. In other words, the combination of BCR engagement by self-antigen and cell-intrinsic PI3K GOF signaling circumvents the need for the requisite second signal to induce activation, thereby facilitating B cell differentiation in response to self-antigen alone.

Strikingly, this break in tolerance results in the generation of both pre-GC plasmablasts and GC B cells, indicating that PI3K is a critical control point for the differentiation of B cells into both of these two populations. Once B cells entered the GC, however, there was selection for B cells expressing BCRs with somatic mutations that decreased affinity for self, indicating that strength of PI3K signaling does not control tolerance within the GC. This clearly delineates the role of PI3K signaling in controlling some, but not all, tolerance checkpoints. This raises the question of what is likely to control immune tolerance within the GC. It might be expected that PI3K-mediated signals downstream of CD40 and IL-21R would mimic the provision of help provided by T cells in the GC; however, clearly these are insufficient to allow selection of autoreactive cells within the GC (Ostiguy et al., 2007; Ren et al., 1994; Zeng et al., 2007).

PI3K signaling can also promote B cell survival (Srinivasan et al., 2009) and thus might be expected to enable survival of self-reactive GC cells. While this does not appear to be the case, it might explain how GC B cells that have mutated their BCR, and consequently no longer bind HEL, continue to survive. This is reminiscent of the survival of B cells that have lost antigen binding in Fas-deficient animals (Butt et al., 2015) and fits with the role of PI3K in protecting against Fas-mediated cell death (Di Cristofano et al., 1999).

Previous work showed that VH4-34–expressing B cells can cross-react with commensal bacteria and that responses to these bacteria may drive autoimmunity (Schickel et al., 2017). Similarly, a recent study of another mouse model of PI3K GOF reported increased B cell responses to commensal bacteria, as well as the presence of IgG autoantibodies that cross-reacted with commensal bacteria, and suggested that this cross-reactivity with bacteria may contribute to the autoimmunity phenomena observed in these mice (Preite et al., 2018). However, we clearly demonstrate that a break in B cell self-tolerance does not require cross-reactivity with foreign antigens, at least for formation of plasmablasts and GCs. It may be that cross-reactivity with commensal organisms, as well as the action of other PI3K GOF cells such as T cells, compounds the effects of the cell-intrinsic break of tolerance and allows the persistence and selection of self-reactive GC B cells as well as driving switching to IgG.

Our findings have several important implications. First, this work predicts that multiple monogenic or polygenic mechanisms that similarly exaggerate PI3K activity could also trigger autoantibody formation. Hence the findings here encourage testing of specific PI3Kδ inhibitors, currently approved for treatment of some human B cell malignancies (Fruman et al., 2017; Hewett et al., 2016) and trialed for treating patients with $PIK3CD$ GOF mutations (Rao et al., 2017), as potential targeted therapies for human antibody-mediated autoimmune diseases. Second, induction of strong PI3K signaling may be beneficial for vaccine responses where some degree of cross-reactivity with self needs to be overcome. Thus, it would be predicted that amplifying PI3K signaling would help initiate immune responses and recruit B cells into the GC, where they could then be selected away from self and toward foreign antigens. Third, our findings resolve the paradox of coexisting clinical features of impaired humoral immune responses to vaccines and natural infection and the development of autoantibody–mediated autoimmunity in patients with $PIK3CD$ GOF mutations. By impairing induction of AID expression and impeding B cell differentiation to plasmablasts, hyperactive p110δ cripples host defense to foreign antigens, thereby explaining poor humoral immunity and immunological memory in patients with $PIK3CD$ GOF mutations (Avery et al., 2018). In contrast, by breaking self-tolerance at the extrafollicular stage of B cell development and activation,

Lau et al.
Activated PI3Kδ breaks B cell tolerance

Journal of Experimental Medicine
https://doi.org/10.1084/jem.20191336

10

hyperactive p110δ enables the generation of autoreactive unmutated plasmablasts producing self-reactive serum IgM. Collectively, our study has provided key insights into the critical role of PI3K in humoral immunity and immune regulation, and how this pathway can both underlie immune pathologies and be targeted for immune modulation in the setting of autoimmune disease and vaccination.

Materials and methods

Human blood samples
Buffy coats from healthy donors were purchased from the Australian Red Cross Blood Service. Peripheral blood and serum samples were collected from patients with *PIK3CD* GOF mutations. Approval for this study was obtained from the human research ethics committees of St. Vincent's Hospital (Sydney, Australia), Sydney South West Area Health Service (Sydney, Australia), Royal Children's Hospital Melbourne (Melbourne, Australia), and the National Institute of Allergy and Infectious Diseases Intramural Institutional Review Board (Bethesda, MD; protocol 96-I-0119); informed consent was obtained from all participants for human experiments in this study.

Mice
HyHEL10-transgenic (SW$_{HEL}$) mice have been previously described (Phan et al., 2003). Specifically, these SW$_{HEL}$ mice were on a CD45.1 congenic (*Ptprc$^{a/a}$*) background and were homozygous for *Rag1* deficiency, resulting in all B cells expressing the HyHEL10 BCR, unable to rearrange their Ig variable region genes (referred to as WT SW$_{HEL}$). *Pik3cd*^{E1020K} have been previously described (Avery et al., 2018). These mice are heterozygous for a G to A base substitution, resulting in a Glu-to-Lys amino acid substitution in p110δ at amino acid residue 1020 (i.e., E1020K; corresponding to E1021K in human p110δ, the most common mutation identified in patients with *PIK3CD* GOF mutations). *Pik3cd*^{E1020K} mice were crossed with *Rag1$^{-/-}$*SW$_{HEL}$ mice to generate *Pik3cd*^{GOF}·*Rag1$^{-/-}$*SW$_{HEL}$ mice (referred to as *Pik3cd*^{GOF} SW$_{HEL}$).

HEL^{3X} is a mutated form of the HEL protein, with R21Q, R73E, and D101R amino acid substitutions (Paus et al., 2006). HEL^{3X} binds to HyHEL10 with an intermediate affinity (equilibrium association constant, $K_a = 1.1 \times 10^7$ M^{-1}). Mice expressing membrane-bound HEL^{3X} on the surface of all cells have been described previously (H3Xtg; Chan et al., 2012).

All mice used in experiments were either generated on a C57BL/6 background (SW$_{HEL}$, *Pik3cd*^{E1020K}, HEL^{3X}) or backcrossed onto a C57BL/6 background >10 times (*Rag1$^{-/-}$*, *Ptprc$^{a/a}$*) and bred at Australian BioResources. C57BL/6 mice were purchased from Australian BioResources. Mice were housed in groups of two to five animals per cage in specific pathogen-free conditions in the Garvan Institute Biological Testing Facility. All experiments were approved by the Garvan Institute-St. Vincent's Animal Ethics Committee. All mice were 6–20 wk old at the start of experiments, unless otherwise stated, and were sex-matched males and females.

Flow cytometry of human samples
Peripheral blood mononuclear cells (PBMCs) from healthy donors and *PIK3CD* GOF patients were stained with anti-CD20 FITC (L27), anti-CD27 PE-Cy7 (M-T271), and anti-CD10 PE (HI10a; all from BD Biosciences), as well as the anti-idiotype antibody 9G4 (IGM Bioscience), which recognizes unmutated VH4-34 antibodies (Potter et al., 1993). Binding of 9G4 to transitional (CD20$^+$CD10$^+$CD27$^-$), naive (CD20$^+$CD10$^-$CD27$^-$), or memory (CD20$^+$CD10$^-$CD27$^+$) B cells was then determined by gating on these B cell populations.

To detect serum VH4-34 antibodies, serum from healthy donors or *PIK3CD* GOF patients was incubated with healthy donor PBMCs for 30 min on ice. Cells were then stained with antibodies against CD20, CD27, and CD10, as well as the 9G4 monoclonal antibody, and the mean fluorescence intensity (MFI) of 9G4 staining on transitional B cells was determined.

Sorting human transitional and naive B cells
PBMCs from healthy donors and *PIK3CD* GOF patients were labeled with antibodies against CD20, CD27, and CD10 as above. Transitional (CD20$^+$CD10$^+$CD27$^-$) or naive (CD20$^+$CD10$^-$CD27$^-$) B cells were then sorted using a FACSAria III (Becton Dickinson; Avery et al., 2018). Purity of the recovered populations was >98%.

Sequencing of human IgM
Amplification of BCR transcripts
IgM transcripts from flow-sorted transitional and naive B cells from six *PIK3CD* GOF patients and nine healthy donors were subjected to massively parallel sequencing. IgM transcripts were amplified, barcoded, pooled, and sequenced on the Illumina MiSeq 2 × 300 bp platform as previously reported (Wang et al., 2018).

Analysis of IGHV usage in BCR repertoires
IGH amplicon libraries were de-multiplexed by matching to index sequence. Paired-end reads were merged using FLASH (Magoč and Salzberg, 2011). *IGHV* and constant region primers were trimmed from the sequences, and any sequence lacking an exact full-length primer match was discarded from the analysis. Trimmed sequences were processed using standalone IgBLAST (Ye et al., 2013) with the IMGT germline reference (Lefranc et al., 2015) to determine the gene segment usage of each transcript. IgM amplicons were confirmed by the presence of the expected IgM CH1 exon sequence. *IGHV* usage frequencies for each subject were calculated for productive B cell lineages, where lineages were inferred from single-linkage clustering at a 90% identity threshold of the CDR3 nucleotide sequences from IGH rearrangements that used the same *IGHV* and *IGHJ* genes (excluding allele) and shared the same CDR3 length (Fu et al., 2012).

Autoantibody arrays
Screening for a broad panel of IgG and IgM autoantibodies was performed using autoantibody arrays (University of Texas Southwestern Medical Center, Genomic and Microarray Core Facility) as described (Li et al., 2007). Briefly, diluted sera were

Lau et al.
Activated PI3Kδ breaks B cell tolerance

Journal of Experimental Medicine
https://doi.org/10.1084/jem.20191336

11

incubated in duplicate with the autoantigen array, and the autoantibodies binding to antigens were detected with Cy3 and Cy5 fluorescently labeled anti-human Ig antibodies (IgG and IgM) generating TIFF images. Genepix Pro 6.0 software was used to analyze the image. Net fluorescence intensity (defined as the spot minus background fluorescence intensity) data obtained from duplicate spots were averaged. Signal-to-noise ratio was used as a quantitative measure of the ability to resolve true signal from background noise, and a signal-to-noise ratio ≥3 was considered a true signal from background noise.

Data were normalized as follows: Ig-positive controls (IgG or IgM) across all samples were averaged, and positive controls in each sample were divided by the averaged positive control, generating a normalization factor for each sample. Each signal was then multiplied by the normalization factor for each block (sample). Values from negative control samples for each antigen were averaged, and ratios were calculated between each sample and the average of negative controls plus two SDs, with values >1 considered positive (Kalantari-Dehaghi et al., 2013). A heatmap of the ratio values was generated using Multi experiment viewer software (Saeed et al., 2003; MeV, Dana-Farber Cancer Institute, Boston, MA), and values were coded as follows: 0, blue; 1, black; 5, yellow. Sera from two patients with SLE were used as positive controls.

Generation of murine BM chimeras
Non–self-reactive and self-reactive BM chimeras were prepared as described (Burnett et al., 2018). Briefly, recipient C57BL/6 or H3Xtg mice (both CD45.2[+] congenic) were given total body irradiation (2× 475 cGy, 6 h apart) using an XRAD 320 Biological Irradiator (Precision X-Ray). After the second dosage, they were reconstituted with 2.5×10^6 BM cells harvested from the femurs and tibias of age- and sex-matched donor mice. BM cells were transferred intravenously in an 80:20 ratio of CD45.1[+]SW$_{HEL}$:CD45.2^{+} cells of the following combinations: WT·SW$_{HEL}$ $Rag1^{-/-}$(CD45.1[+]): C57BL/6(CD45.2[+]) into C57BL/6 recipients, $Pik3cd^{GOF}$·SW$_{HEL}$ $Rag1^{-/-}$(CD45.1[+]): C57BL/6(CD45.2[+]) into C57BL/6 recipients, WT·SW$_{HEL}$ $Rag1^{-/-}$(CD45.1[+]):H3Xtg(CD45.2[+]) into H3Xtg recipients, and $Pik3cd^{GOF}$·SW$_{HEL}$ $Rag1^{-/-}$(CD45.1[+]):H3Xtg (CD45.2[+]) into H3Xtg recipients. Mice were allowed to reconstitute for 8–15 wk in the same cage groups.

Flow cytometry of BM chimeric mice
BM, spleens, and sera of the BM chimeras were harvested 8–15 wk after reconstitution. Single-cell suspensions of the BM and spleen were prepared and stained with antibodies for flow cytometry. HEL-binding cells were detected by staining cells with HEL (Sigma-Aldrich), followed by secondary staining with HyHEL9 (University of California San Francisco Monoclonal Antibody Core) conjugated to Alexa Fluor 647 (Invitrogen; Brink et al., 2015), along with other relevant antibodies. Data were acquired on the LSRII Fortessa (BD Biosciences). Analysis was conducted using FlowJo software (Tree Star). All data are representative of five or more experiments, with n = 2–3 of each chimera combination per experiment.

The following antibodies were purchased from BD Biosciences: anti-CD43 PE (S7), anti-CD45.2 BUV395 (104), anti-CD45R/B220 BV786, anti-CD19 BV510 (1D3), anti-CD95 PE (Jo2), biotinylated anti-CD138 (281–2), anti-CD16/CD32 Fc block (2.4G2), anti-IgM PE (AF6-78), biotinylated anti-IgM (AF6-78), and streptavidin-BV711. The following were purchased from eBioscience: anti-CD23 PeCy7 (B3B4) and anti-CD93 PE (AA4.1). The following were purchased from Biolegend: anti-IgD APC-Cy7 (11-26c.2a), anti-CD24 PB (M1/69), anti-CD38 PE-Cy7 (90), anti-CD86 BV650 (GL-1), anti-CD93 PerCP-Cy5.5 (AA4.1), and anti-CD21/35 PB (7E9). The following was purchased from Invitrogen: anti-CD45.1 FITC (A20). HEL^{WT} was purchased from Sigma-Aldrich.

ELISA
Serum concentrations of HEL-specific IgM, IgG1, IgG2a, IgG2b, and IgG3 antibodies were determined using ELISA, as described (Brink et al., 2015). 96-well ELISA plates (Nunc) were coated with HEL^{WT} overnight. Plates were then incubated with serum samples. Serum Igs bound to the plates were quantified using biotinylated IgH chain isotype-specific antibodies, followed by incubation with streptavidin-alkaline phosphatase (Amersham). Plates were then developed using p-nitrophenyl phosphate substrate. Ig levels for each class were quantified with HyHEL10 standards. All data are representative of seven or more experiments, with n = 2–3 of each chimera combination per experiment.

The following antibodies were purchased from BD Biosciences: biotinylated anti-IgG1 (A85-1), biotinylated anti-IgG2a [b] (5.7), biotinylated anti-IgG2b (RMG2b-1), and biotinylated anti-IgG3 (R40-82). The following was purchased from Jackson ImmunoResearch: biotinylated anti-IgM.

In vitro stimulation
Fresh spleen cell preparations from BM chimeric mice underwent RBC lysis and were cultured for 18 h at 37°C in B cell media (RPMI-1640 [Invitrogen], 10% FBS [GE Healthcare], 5.5×10^{-5} M 2-mercaptoethanol [Sigma-Aldrich], 10 mM Hepes [Gibco], 100 µg/ml normocin [InvivoGen], 1 mM sodium pyruvate [Gibco], 100 U/ml penicillin [Thermo Fisher Scientific], and MEM nonessential amino acids [Sigma-Aldrich]), alone or with HEL^{WT} (200 ng/ml). Cells were then harvested and stained to detect surface CD86 expression on SW$_{HEL}$ cells by flow cytometry.

SW$_{HEL}$ BCR sequencing
Cell suspensions were prepared as for flow cytometric analysis. SW$_{HEL}$ GC cells, plasmablasts (Fig. 4), and non-GC cells (Fas^{lo}CD38^{hi}) from $Pik3cd^{GOF}$·SW$_{HEL}$ $Rag1^{-/-}$:H3Xtg chimeras were single-cell sorted into 96-well plates (Thermo Fisher Scientific) using a FACSAriaIII (BD Biosciences). Each well contained 10× Taq Buffer (Invitrogen), 10 mg/ml proteinase K (Promega), 10% Tween-20, 10 mM Na$_2$EDTA, and distilled H$_2$O (Baxter) in a total volume of 10 µl. Proteinase K digestion was performed by heating plates to 56°C for 40 min, followed by 95°C for 8 min. PCR was then performed with Taq DNA polymerase (Invitrogen) and deoxyribonucleotide triphosphates (Sigma-

Lau et al.
Activated PI3Kδ breaks B cell tolerance

Journal of Experimental Medicine
https://doi.org/10.1084/jem.20191336

12

Aldrich). For primary PCR, HyHEL10 primary forward and reverse sequencing primers were used. Primary PCR conditions were as follows: 94°C for 3 min, followed by 34 cycles of 95°C for 15 s, 55°C for 1 min, and 72°C for 1 min. A 1:10 dilution of the primary PCR product was then transferred into a fresh 96-well plate for secondary PCR. For secondary PCR, HyHEL10 secondary forward and reverse sequencing primers were used. Secondary PCR conditions were as follows: 94°C for 3 min, followed by 35 cycles of 95°C for 15 s, 62°C for 40 s, and 72°C for 1 min. PCR product purity was determined using SYBR Safe DNA gel staining (Thermo Fisher Scientific). Sanger sequencing was performed by Genewiz.

Quantification and statistical analysis

The exact values of n indicating the total number of human samples or animals per group, as well as the definition of center, dispersion, and precision measures are indicated in each figure and figure legend. Significant differences were determined using Prism (GraphPad Software). For comparisons between two groups, significant differences were determined by Mann-Whitney or two-tailed t test (Figs. 1, 2, and 7). For multiple comparisons, two-way ANOVA was used (Figs. 3, 4, 5, and 6). Asterisks indicate statistical significance (*, $P < 0.05$; **, $P < 0.01$; ***, $P < 0.001$; ****, $P < 0.0001$). Significant differences for each antigen between healthy donors and patients carrying the *PIK3CD* GOF mutation were determined using the significance analysis for microarrays test with a false discovery rate of 3%.

Online supplemental material

Fig. S1 shows the binding of both human IgM and IgG serum antibodies to the entire autoantigen array. Fig. S2 shows the *IGHV* gene segment usage in B cell clonal lineages from the transitional and naive compartments of healthy donors and *PIK3CD* GOF patients. Fig. S3 shows gating in the spleen for SW$_{HEL}$ cells, gating and percentages of transitional cells, absolute numbers of SW$_{HEL}$ populations in the spleen, and CD1d expression on SW$_{HEL}$ cells. Fig. S4 shows IgD expression and HEL binding of SW$_{HEL}$ cells. Fig. S5 shows levels of serum anti-HEL IgG isotypes and mixed BM chimeras.

References

Akerlund, J., A. Getahun, and J.C. Cambier. 2015. B cell expression of the SH2-containing inositol 5-phosphatase (SHIP-1) is required to establish anergy to high affinity, proteinaceous autoantigens. *J. Autoimmun.* 62: 45–54. https://doi.org/10.1016/j.jaut.2015.06.007

Angulo, I., O. Vadas, F. Garçon, E. Banham-Hall, V. Plagnol, T.R. Leahy, H. Baxendale, T. Coulter, J. Curtis, C. Wu, et al. 2013. Phosphoinositide 3-kinase δ gene mutation predisposes to respiratory infection and airway damage. *Science.* 342:866–871. https://doi.org/10.1126/science.1243292

Avery, D.T., A. Kane, T. Nguyen, A. Lau, A. Nguyen, H. Lenthall, K. Payne, W. Shi, H. Brigden, E. French, et al. 2018. Germline-activating mutations in *PIK3CD* compromise B cell development and function. *J. Exp. Med.* 215: 2073–2095. https://doi.org/10.1084/jem.20180010

Bier, J., G. Rao, K. Payne, H. Brigden, E. French, S.J. Pelham, A. Lau, H. Lenthall, E.S.J. Edwards, J.M. Smart, et al. 2019. Activating mutations in PIK3CD disrupt the differentiation and function of human and murine CD4⁺ T cells. *J. Allergy Clin. Immunol.* 144:236–253. https://doi.org/10.1016/j.jaci.2019.01.033

Bleesing, J.J.H., and T.A. Fleisher. 2003. Human B cells express a CD45 isoform that is similar to murine B220 and is downregulated with acquisition of the memory B-cell marker CD27. *Cytometry B Clin. Cytom.* 51: 1–8. https://doi.org/10.1002/cyto.b.10007

Brink, R., and T.G. Phan. 2018. Self-reactive B cells in the germinal center reaction. *Annu. Rev. Immunol.* 36:339–357. https://doi.org/10.1146/annurev-immunol-051116-052510

Brink, R., D. Paus, K. Bourne, J.R. Hermes, S. Gardam, T.G. Phan, and T.D. Chan. 2015. The SW$_{(HEL)}$ system for high-resolution analysis of in vivo antigen-specific T-dependent B cell responses. *Methods Mol. Biol.* 1291: 103–123. https://doi.org/10.1007/978-1-4939-2498-1_9

Browne, C.D., C.J. Del Nagro, M.H. Cato, H.S. Dengler, and R.C. Rickert. 2009. Suppression of phosphatidylinositol 3,4,5-trisphosphate production is a key determinant of B cell anergy. *Immunity.* 31:749–760. https://doi.org/10.1016/j.immuni.2009.08.026

Burnett, D.L., D.B. Langley, P. Schofield, J.R. Hermes, T.D. Chan, J. Jackson, K. Bourne, J.H. Reed, K. Patterson, B.T. Porebski, et al. 2018. Germinal center antibody mutation trajectories are determined by rapid self/foreign discrimination. *Science.* 360:223–226. https://doi.org/10.1126/science.aao3859

Butt, D., T.D. Chan, K. Bourne, J.R. Hermes, A. Nguyen, A. Statham, L.A. O'Reilly, A. Strasser, S. Price, P. Schofield, et al. 2015. FAS inactivation releases unconventional germinal center B cells that escape antigen control and drive IgE and autoantibody production. *Immunity.* 42: 890–902. https://doi.org/10.1016/j.immuni.2015.04.010

Cannons, J.L., S. Preite, S.M. Kapnick, G. Uzel, and P.L. Schwartzberg. 2018. Genetic defects in phosphoinositide 3-kinase δ influence CD8⁺ T cell survival, differentiation, and function. *Front. Immunol.* 9:1758. https://doi.org/10.3389/fimmu.2018.01758

Cappione, A.J., A.E. Pugh-Bernard, J.H. Anolik, and I. Sanz. 2004. Lupus IgG VH4.34 antibodies bind to a 220-kDa glycoform of CD45/B220 on the surface of human B lymphocytes. *J. Immunol.* 172:4298–4307. https://doi.org/10.4049/jimmunol.172.7.4298

Chan, T.D., K. Wood, J.R. Hermes, D. Butt, C.J. Jolly, A. Basten, and R. Brink. 2012. Elimination of germinal-center-derived self-reactive B cells is governed by the location and concentration of self-antigen. *Immunity.* 37:893–904. https://doi.org/10.1016/j.immuni.2012.07.017

Cooke, M.P., A.W. Heath, K.M. Shokat, Y. Zeng, F.D. Finkelman, P.S. Linsley, M. Howard, and C.C. Goodnow. 1994. Immunoglobulin signal transduction guides the specificity of B cell-T cell interactions and is blocked in tolerant self-reactive B cells. *J. Exp. Med.* 179:425–438. https://doi.org/10.1084/jem.179.2.425

Coulter, T.I., A. Chandra, C.M. Bacon, J. Babar, J. Curtis, N. Screaton, J.R. Goodlad, G. Farmer, C.L. Steele, T.R. Leahy, et al. 2017. Clinical spectrum and features of activated phosphoinositide 3-kinase δ syndrome: A large patient cohort study. *J. Allergy Clin. Immunol.* 139:597–606.e4. https://doi.org/10.1016/j.jaci.2016.06.021

Crank, M.C., J.K. Grossman, S. Moir, S. Pittaluga, C.M. Buckner, L. Kardava, A. Agharahimi, H. Meuwissen, J. Stoddard, J. Niemela, et al. 2014. Mutations in PIK3CD can cause hyper IgM syndrome (HIGM) associated with increased cancer susceptibility. *J. Clin. Immunol.* 34:272–276. https://doi.org/10.1007/s10875-014-0012-9

Cura Daball, P., M.S. Ventura Ferreira, S. Ammann, C. Klemann, M.R. Lorenz, U. Warthorst, T.R. Leahy, N. Conlon, J. Roche, P. Soler-Palacín, et al. 2018. CD57 identifies T cells with functional senescence before terminal differentiation and relative telomere shortening in patients with activated PI3 kinase delta syndrome. *Immunol. Cell Biol.* 96:1060–1071. https://doi.org/10.1111/imcb.12169

Di Cristofano, A., P. Kotsi, Y.F. Peng, C. Cordon-Cardo, K.B. Elkon, and P.P. Pandolfi. 1999. Impaired Fas response and autoimmunity in Pten$^{+/-}$ mice. *Science.* 285:2122–2125. https://doi.org/10.1126/science.285.5436.2122

Durand, C.A., K. Hartvigsen, L. Fogelstrand, S. Kim, S. Iritani, B. Vanhaesebroeck, J.L. Witztum, K.D. Puri, and M.R. Gold. 2009. Phosphoinositide 3-kinase p110 δ regulates natural antibody production, marginal zone and B-1 B cell function, and autoantibody responses. *J. Immunol.* 183:5673–5684. https://doi.org/10.4049/jimmunol.0900432

Edwards, E.S.J., J. Bier, T.S. Cole, M. Wong, P. Hsu, L.J. Berglund, K. Boztug, A. Lau, E. Gostick, D.A. Price, et al. 2019. Activating PIK3CD mutations impair human cytotoxic lymphocyte differentiation and function and EBV immunity. *J. Allergy Clin. Immunol.* 143:276–291.e6. https://doi.org/10.1016/j.jaci.2018.04.030

Eris, J.M., A. Basten, R. Brink, K. Doherty, M.R. Kehry, and P.D. Hodgkin. 1994. Anergic self-reactive B cells present self antigen and respond normally to CD40-dependent T-cell signals but are defective in antigen-receptor-mediated functions. *Proc. Natl. Acad. Sci. USA.* 91:4392–4396. https://doi.org/10.1073/pnas.91.10.4392

Fruman, D.A., H. Chiu, B.D. Hopkins, S. Bagrodia, L.C. Cantley, and R.T. Abraham. 2017. The PI3K pathway in human disease. *Cell.* 170:605–635. https://doi.org/10.1016/j.cell.2017.07.029

Fu, L., B. Niu, Z. Zhu, S. Wu, and W. Li. 2012. CD-HIT: accelerated for clustering the next-generation sequencing data. *Bioinformatics.* 28:3150–3152. https://doi.org/10.1093/bioinformatics/bts565

Getahun, A., N.A. Beavers, S.R. Larson, M.J. Shlomchik, and J.C. Cambier. 2016. Continuous inhibitory signaling by both SHP-1 and SHIP-1 pathways is required to maintain unresponsiveness of anergic B cells. *J. Exp. Med.* 213:751–769. https://doi.org/10.1084/jem.20150537

Goodnow, C.C., J. Crosbie, S. Adelstein, T.B. Lavoie, S.J. Smith-Gill, R.A. Brink, H. Pritchard-Briscoe, J.S. Wotherspoon, R.H. Loblay, K. Raphael, et al. 1988. Altered immunoglobulin expression and functional silencing of self-reactive B lymphocytes in transgenic mice. *Nature.* 334:676–682. https://doi.org/10.1038/334676a0

Goodnow, C.C., J. Sprent, B. Fazekas de St Groth, and C.G. Vinuesa. 2005. Cellular and genetic mechanisms of self tolerance and autoimmunity. *Nature.* 435:590–597. https://doi.org/10.1038/nature03724

Greaves, S.A., J.N. Peterson, P. Strauch, R.M. Torres, and R. Pelanda. 2019. Active PI3K abrogates central tolerance in high-avidity autoreactive B cells. *J. Exp. Med.* 216:1135–1153. https://doi.org/10.1084/jem.20181652

Hayter, S.M., and M.C. Cook. 2012. Updated assessment of the prevalence, spectrum and case definition of autoimmune disease. *Autoimmun. Rev.* 11:754–765. https://doi.org/10.1016/j.autrev.2012.02.001

Hewett, Y.G., D. Uprety, and B.K. Shah. 2016. Idelalisib- a PI3Kδ targeting agent for B-cell malignancies. *J. Oncol. Pharm. Pract.* 22:284–288. https://doi.org/10.1177/1078155215572933

Inaoki, M., S. Sato, B.C. Weintraub, C.C. Goodnow, and T.F. Tedder. 1997. CD19-regulated signaling thresholds control peripheral tolerance and autoantibody production in B lymphocytes. *J. Exp. Med.* 186:1923–1931. https://doi.org/10.1084/jem.186.11.1923

Kalantari-Dehaghi, M., G.J. Anhalt, M.J. Camilleri, A.I. Chernyavsky, S. Chun, P.L. Felgner, A. Jasinskas, K.M. Leiferman, L. Liang, S. Marchenko, et al. 2013. Pemphigus vulgaris autoantibody profiling by proteomic technique. *PLoS One.* 8:e57587. https://doi.org/10.1371/journal.pone.0057587

Lefranc, M.P., V. Giudicelli, P. Duroux, J. Jabado-Michaloud, G. Folch, S. Aouinti, E. Carillon, H. Duvergey, A. Houles, T. Paysan-Lafosse, et al. 2015. IMGT®, the international ImMunoGeneTics information system® 25 years on. *Nucleic Acids Res.* 43(D1):D413–D422. https://doi.org/10.1093/nar/gku1056

Leung, W.-H., T. Tarasenko, Z. Biesova, H. Kole, E.R. Walsh, and S. Bolland. 2013. Aberrant antibody affinity selection in SHIP-deficient B cells. *Eur. J. Immunol.* 43:371–381. https://doi.org/10.1002/eji.201242809

Li, Q.Z., J. Zhou, A.E. Wandstrat, F. Carr-Johnson, V. Branch, D.R. Karp, C. Mohan, E.K. Wakeland, and N.J. Olsen. 2007. Protein array autoantibody profiles for insights into systemic lupus erythematosus and incomplete lupus syndromes. *Clin. Exp. Immunol.* 147:60–70.

Lucas, C.L., H.S. Kuehn, F. Zhao, J.E. Niemela, E.K. Deenick, U. Palendira, D.T. Avery, L. Moens, J.L. Cannons, M. Biancalana, et al. 2014. Dominant-activating germline mutations in the gene encoding the PI(3)K catalytic subunit p110δ result in T cell senescence and human immunodeficiency. *Nat. Immunol.* 15:88–97. https://doi.org/10.1038/ni.2771

Maccari, M.E., H. Abolhassani, A. Aghamohammadi, A. Aiuti, O. Aleinikova, C. Bangs, S. Baris, F. Barzaghi, H. Baxendale, M. Buckland, et al. 2018. Disease evolution and response to rapamycin in activated phosphoinositide 3-kinase δ syndrome: the European Society for Immunodeficiencies-Activated Phosphoinositide 3-Kinase δ Syndrome Registry. *Front. Immunol.* 9:543. https://doi.org/10.3389/fimmu.2018.00543

Magoč, T., and S.L. Salzberg. 2011. FLASH: fast length adjustment of short reads to improve genome assemblies. *Bioinformatics.* 27:2957–2963. https://doi.org/10.1093/bioinformatics/btr507

Nemazee, D. 2017. Mechanisms of central tolerance for B cells. *Nat. Rev. Immunol.* 17:281–294. https://doi.org/10.1038/nri.2017.19

O'Neill, S.K., A. Getahun, S.B. Gauld, K.T. Merrell, I. Tamir, M.J. Smith, J.M. Dal Porto, Q.-Z. Li, and J.C. Cambier. 2011. Monophosphorylation of CD79a and CD79b ITAM motifs initiates a SHIP-1 phosphatase-mediated inhibitory signaling cascade required for B cell anergy. *Immunity.* 35:746–756. https://doi.org/10.1016/j.immuni.2011.10.011

Okkenhaug, K. 2013. Signaling by the phosphoinositide 3-kinase family in immune cells. *Annu. Rev. Immunol.* 31:675–704. https://doi.org/10.1146/annurev-immunol-032712-095946

Ostiguy, V., E.-L. Allard, M. Marquis, J. Leignadier, and N. Labrecque. 2007. IL-21 promotes T lymphocyte survival by activating the phosphatidylinositol-3 kinase signaling cascade. *J. Leukoc. Biol.* 82:645–656. https://doi.org/10.1189/jlb.0806494

Paus, D., T.G. Phan, T.D. Chan, S. Gardam, A. Basten, and R. Brink. 2006. Antigen recognition strength regulates the choice between extra-follicular plasma cell and germinal center B cell differentiation. *J. Exp. Med.* 203:1081–1091. https://doi.org/10.1084/jem.20060087

Phan, T.G., M. Amesbury, S. Gardam, J. Crosbie, J. Hasbold, P.D. Hodgkin, A. Basten, and R. Brink. 2003. B cell receptor-independent stimuli trigger immunoglobulin (Ig) class switch recombination and production of IgG autoantibodies by anergic self-reactive B cells. *J. Exp. Med.* 197:845–860. https://doi.org/10.1084/jem.20022144

Phan, T.G., D. Paus, T.D. Chan, M.L. Turner, S.L. Nutt, A. Basten, and R. Brink. 2006. High affinity germinal center B cells are actively selected into the plasma cell compartment. *J. Exp. Med.* 203:2419–2424. https://doi.org/10.1084/jem.20061254

Potter, K.N., Y. Li, V. Pascual, R.C. Williams Jr., L.C. Byres, M. Spellerberg, F.K. Stevenson, and J.D. Capra. 1993. Molecular characterization of a cross-reactive idiotype on human immunoglobulins utilizing the VH4-21 gene segment. *J. Exp. Med.* 178:1419–1428. https://doi.org/10.1084/jem.178.4.1419

Preite, S., J.L. Cannons, A.J. Radtke, I. Vujkovic-Cvijin, J. Gomez-Rodriguez, S. Volpi, B. Huang, J. Cheng, N. Collins, J. Reilley, et al. 2018. Hyperactivated PI3Kδ promotes self and commensal reactivity at the expense of optimal humoral immunity. *Nat. Immunol.* 19:986–1000. https://doi.org/10.1038/s41590-018-0182-3

Preite, S., B. Huang, J.L. Cannons, D.B. McGavern, and P.L. Schwartzberg. 2019. PI3K orchestrates T follicular helper cell differentiation in a context dependent manner: implications for autoimmunity. *Front. Immunol.* 9:3079. https://doi.org/10.3389/fimmu.2018.03079

Pugh-Bernard, A.E., G.J. Silverman, A.J. Cappione, M.E. Villano, D.H. Ryan, R.A. Insel, and I. Sanz. 2001. Regulation of inherently autoreactive VH4-

34 B cells in the maintenance of human B cell tolerance. *J. Clin. Invest.* 108:1061–1070. https://doi.org/10.1172/JCI200112462

Rao, V.K., S. Webster, V.A.S.H. Dalm, A. Šedivá, P.M. van Hagen, S. Holland, S.D. Rosenzweig, A.D. Christ, B. Sloth, M. Cabanski, et al. 2017. Effective "activated PI3Kδ syndrome"-targeted therapy with the PI3Kδ inhibitor leniolisib. *Blood.* 130:2307–2316. https://doi.org/10.1182/blood-2017-08-801191

Ren, C.L., T. Morio, S.M. Fu, and R.S. Geha. 1994. Signal transduction via CD40 involves activation of lyn kinase and phosphatidylinositol-3-kinase, and phosphorylation of phospholipase C gamma 2. *J. Exp. Med.* 179:673–680. https://doi.org/10.1084/jem.179.2.673

Ruiz-García, R., A. Vargas-Hernández, I.K. Chinn, L.S. Angelo, T.N. Cao, Z. Coban-Akdemir, S.N. Jhangiani, Q. Meng, L.R. Forbes, D.M. Muzny, et al. 2018. Mutations in PI3K110δ cause impaired natural killer cell function partially rescued by rapamycin treatment. *J. Allergy Clin. Immunol.* 142:605–617.e7. https://doi.org/10.1016/j.jaci.2017.11.042

Saeed, A.I., V. Sharov, J. White, J. Li, W. Liang, N. Bhagabati, J. Braisted, M. Klapa, T. Currier, M. Thiagarajan, et al. 2003. TM4: a free, open-source system for microarray data management and analysis. *Biotechniques.* 34:374–378. https://doi.org/10.2144/03342mt01

Schickel, J.-N., S. Glauzy, Y.-S. Ng, N. Chamberlain, C. Massad, I. Isnardi, N. Katz, G. Uzel, S.M. Holland, C. Picard, et al. 2017. Self-reactive VH4-34-expressing IgG B cells recognize commensal bacteria. *J. Exp. Med.* 214:1991–2003. https://doi.org/10.1084/jem.20160201

Setz, C.S., A. Khadour, V. Renna, J. Iype, E. Gentner, X. He, M. Datta, M. Young, L. Nitschke, J. Wienands, et al. 2019. Pten controls B-cell responsiveness and germinal center reaction by regulating the expression of IgD BCR. *EMBO J.* 38:e100249. https://doi.org/10.15252/embj.2018100249

Shlomchik, M.J. 2008. Sites and stages of autoreactive B cell activation and regulation. *Immunity.* 28:18–28. https://doi.org/10.1016/j.immuni.2007.12.004

Smith, M.J., B.R. Ford, M. Rihanek, B.M. Coleman, A. Getahun, V.D. Sarapura, P.A. Gottlieb, and J.C. Cambier. 2019. Elevated PTEN expression maintains anergy in human B cells and reveals unexpectedly high repertoire autoreactivity. *JCI Insight.* 4:e123384. https://doi.org/10.1172/jci.insight.123384

Srinivasan, L., Y. Sasaki, D.P. Calado, B. Zhang, J.-H. Paik, R.A. DePinho, J.L. Kutok, J.F. Kearney, K.L. Otipoby, and K. Rajewsky. 2009. PI3 kinase signals BCR-dependent mature B cell survival. *Cell.* 139:573–586. https://doi.org/10.1016/j.cell.2009.08.041

Stark, A.-K., A. Chandra, K. Chakraborty, R. Alam, V. Carbonaro, J. Clark, S. Sriskantharajah, G. Bradley, A.G. Richter, E. Banham-Hall, et al. 2018. PI3Kδ hyper-activation promotes development of B cells that exacerbate Streptococcus pneumoniae infection in an antibody-independent manner. *Nat. Commun.* 9:3174. https://doi.org/10.1038/s41467-018-05674-8

Taylor, D.K., E. Ito, M. Thorn, K. Sundar, T. Tedder, and L.A. Spatz. 2006. Loss of tolerance of anti-dsDNA B cells in mice overexpressing CD19. *Mol. Immunol.* 43:1776–1790. https://doi.org/10.1016/j.molimm.2005.11.003

Wang, J.J., J.H. Reed, A.D. Colella, A.J. Russell, W. Murray-Brown, T.K. Chataway, K.J.L. Jackson, C.C. Goodnow, and T.P. Gordon. 2018. Molecular profiling and clonal tracking of secreted rheumatoid factors in primary Sjögren's syndrome. *Arthritis Rheumatol.* 70:1617–1625. https://doi.org/10.1002/art.40539

Wardemann, H., S. Yurasov, A. Schaefer, J.W. Young, E. Meffre, and M.C. Nussenzweig. 2003. Predominant autoantibody production by early human B cell precursors. *Science.* 301:1374–1377. https://doi.org/10.1126/science.1086907

Wentink, M., V. Dalm, A.C. Lankester, P.A. van Schouwenburg, L. Schölvinck, T. Kalina, R. Zachova, A. Sediva, A. Lambeck, I. Pico-Knijnenburg, et al. 2017. Genetic defects in PI3Kδ affect B-cell differentiation and maturation leading to hypogammaglobulineamia and recurrent infections. *Clin. Immunol.* 176:77–86. https://doi.org/10.1016/j.clim.2017.01.004

Wentink, M.W.J., Y.M. Mueller, V.A.S.H. Dalm, G.J. Driessen, P.M. van Hagen, J.M. van Montfrans, M. van der Burg, and P.D. Katsikis. 2018. Exhaustion of the CD8+ T cell compartment in patients with mutations in phosphoinositide 3-kinase delta. *Front. Immunol.* 9:446. https://doi.org/10.3389/fimmu.2018.00446

Wray-Dutra, M.N., F. Al Qureshah, G. Metzler, M. Oukka, R.G. James, and D.J. Rawlings. 2018. Activated PIK3CD drives innate B cell expansion yet limits B cell-intrinsic immune responses. *J. Exp. Med.* 215:2485–2496. https://doi.org/10.1084/jem.20180617

Ye, J., N. Ma, T.L. Madden, and J.M. Ostell. 2013. IgBLAST: an immunoglobulin variable domain sequence analysis tool. *Nucleic Acids Res.* 41(W1):W34-40. https://doi.org/10.1093/nar/gkt382

Zeng, R., R. Spolski, E. Casas, W. Zhu, D.E. Levy, and W.J. Leonard. 2007. The molecular basis of IL-21-mediated proliferation. *Blood.* 109:4135–4142. https://doi.org/10.1182/blood-2006-10-054973

Supplemental material

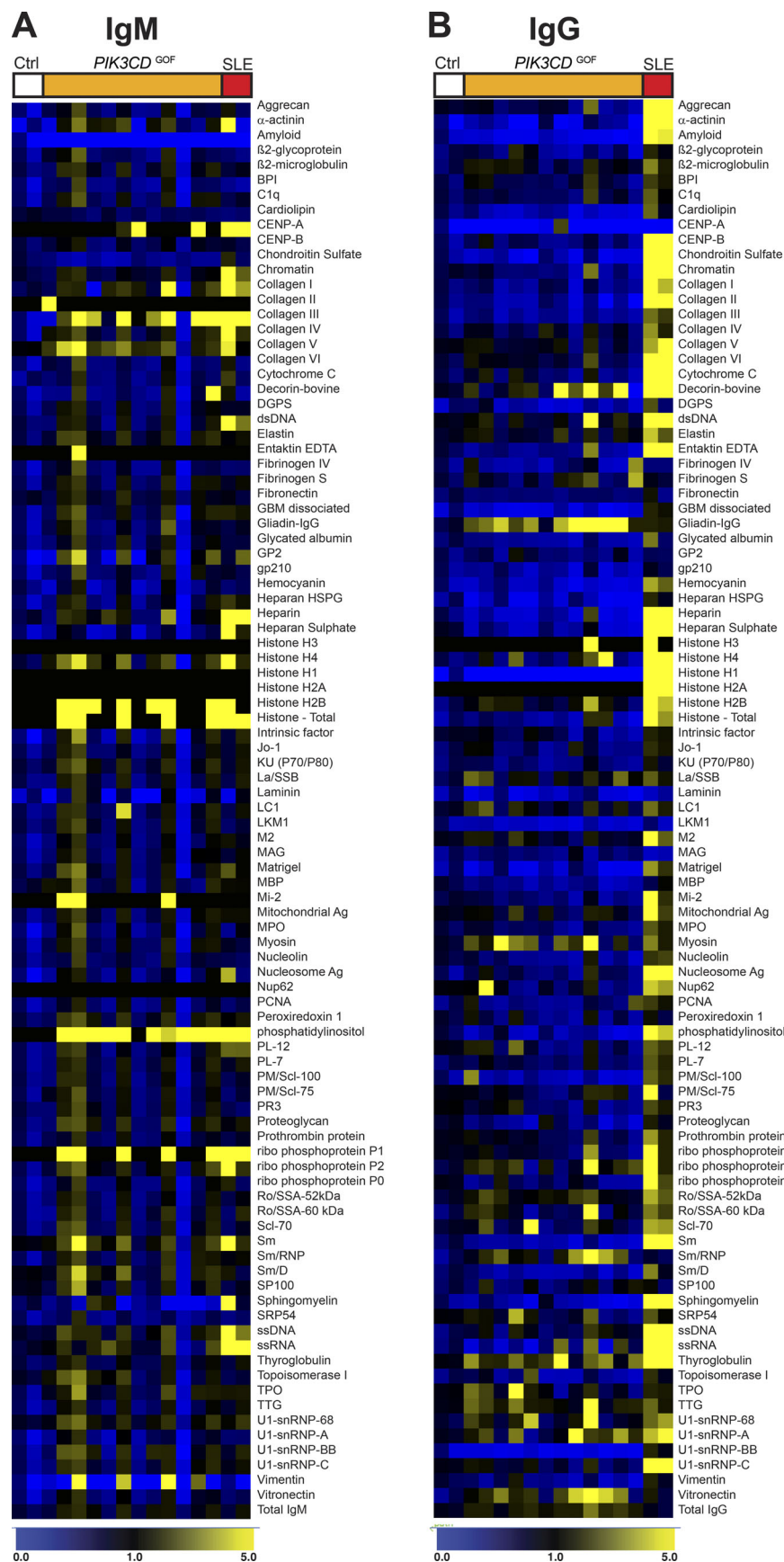**Lau et al., https://doi.org/10.1084/jem.20191336**

Figure S1. **Autoantibodies in serum of *PIK3CD* GOF patients. (A and B)** Heatmap showing relative binding of serum IgM (A) and IgG (B) from healthy controls (Ctrl; *n* = 2), *PIK3CD* GOF (*n* = 12), and SLE (*n* = 2) patients to a full array of different self-antigens. dsDNA, double-stranded DNA.
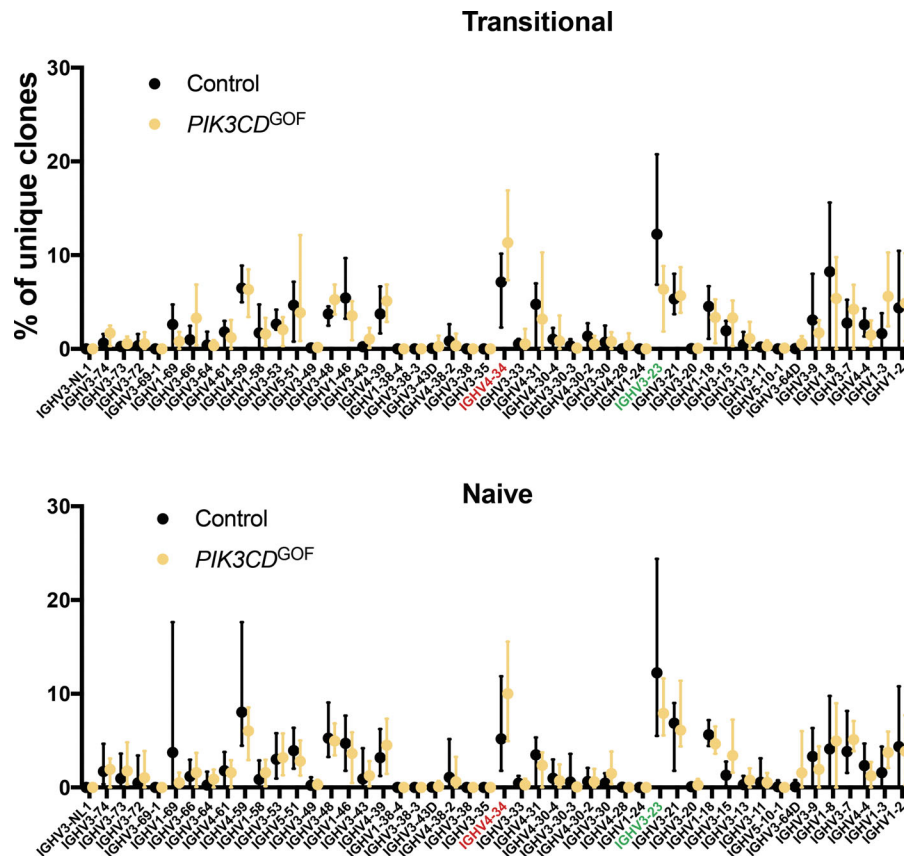
Figure S2. **BCRs using the autoreactive IGHV4-34 heavy chain are enriched in the IgM repertoire of *PIK3CD* GOF patients.** *IGHV* gene segment usage in B cell clonal lineages from the transitional and naive compartments of healthy donors (black; *n* = 8–9) and *PIK3CD* GOF patients (yellow; *n* = 6). Points show mean *IGHV* segment usage in transitional (top panel) or naive (bottom panel) B cells. Lines extending from points indicate the minimum and maximum utilization for each *IGHV* gene segment within each group. *IGHV* genes on the x axis are ordered for their chromosomal position in the *IGH* locus from *IGHJ* distal to proximal (left to right), with unmapped genes on the left. Significant decreases were found in the usage of *IGHV3-23* (shown in green) in patients (transitional adjusted P = 2.13 × 10^{-7}; naive adjusted P = 0.0221; ANOVA Tukey honest significant difference post-test).
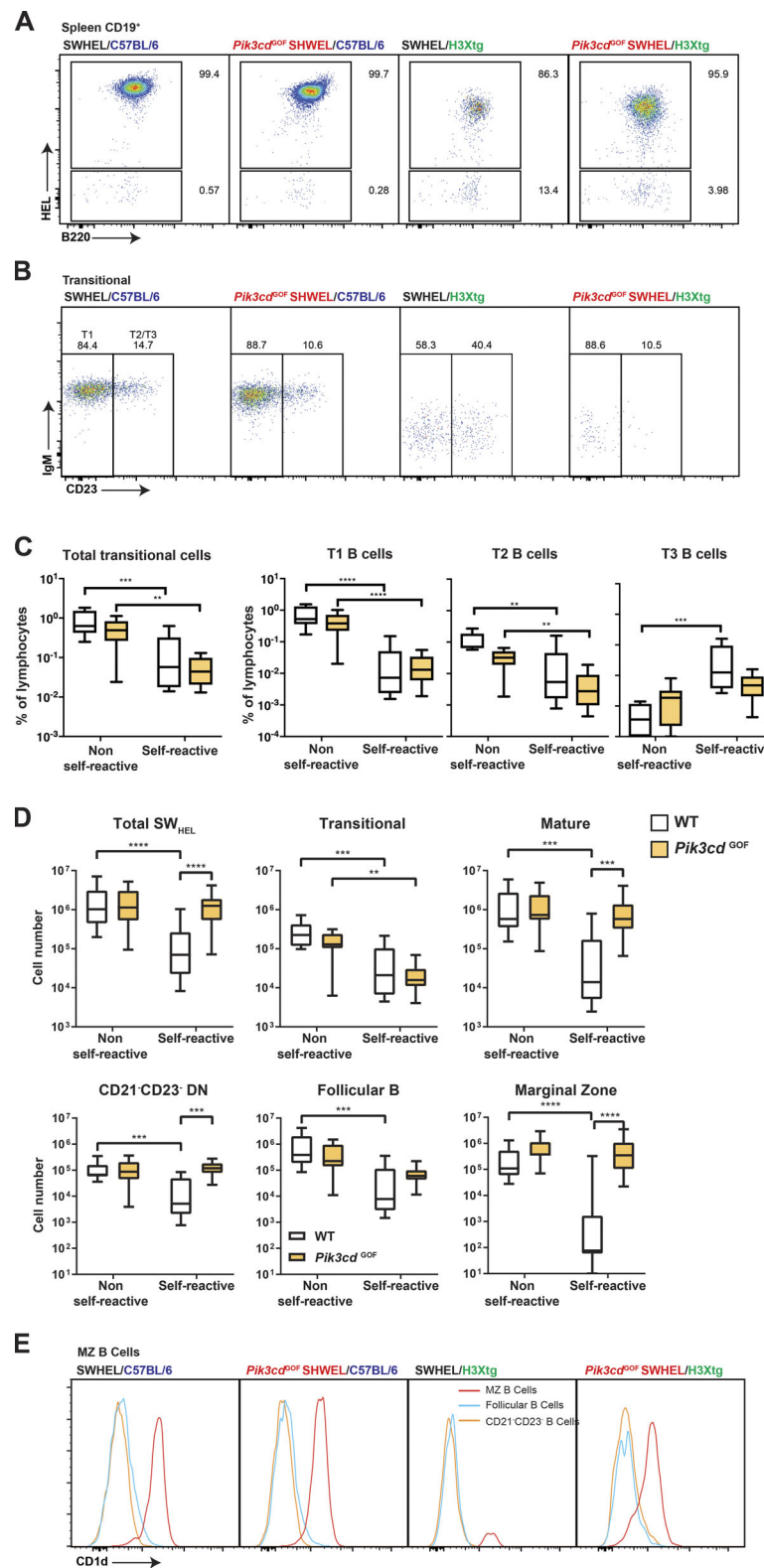
Figure S3.   Flow cytometry and gating of splenic B cell populations. Spleens were harvested from BM chimeras as in Fig. 4. **(A and B)** Representative staining and gating is shown for CD45.1$^+$CD19$^+$ cells showing gating for HEL binders (A) and for HEL binders showing gating of transitional (CD93$^+$) B cells for T1 (CD23$^-$) and T2/T3 (CD23$^+$) subsets (B). **(C)** Percentages of total transitional and each transitional population. The center line shows the median, box limits show the upper and lower quartiles, and whiskers show the minimum and maximum (n = 8–9 combined from five experiments). **(D)** Absolute numbers of different populations. The center line shows the median, box limits show the upper and lower quartiles, and whiskers show the minimum and maximum (n = 8–17 combined from five to eight experiments). **(E)** CD1d expression on different mature B cell populations, with representative staining from four different experiments. **, P < 0.01; ***, P < 0.001; ****, P < 0.0001.
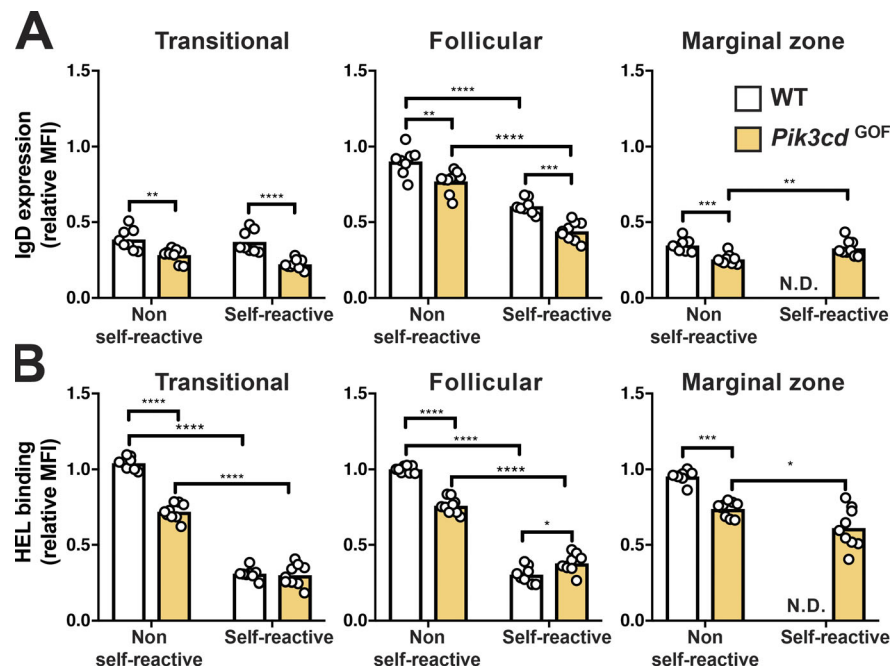
Figure S4. **Antigen receptor expression on self-reactive B cells. (A)** Expression of IgD on transitional, follicular, and MZ SW$_{HEL}$ cells. Values are expressed relative to IgD expression on WT CD45.2$^+$ follicular cells. **(B)** HEL binding of SW$_{HEL}$ cells. Values are shown relative to HEL binding of WT SW$_{HEL}$ cells in a non–self-reactive environment. Each point represents a different mouse, and bars show means (n = 8–9 combined from five experiments). N.D., not done, as insufficient numbers of MZ cells were generated to be confidently analyzed. *, P < 0.05; **, P < 0.01; ***, P < 0.001; ****, P < 0.0001.
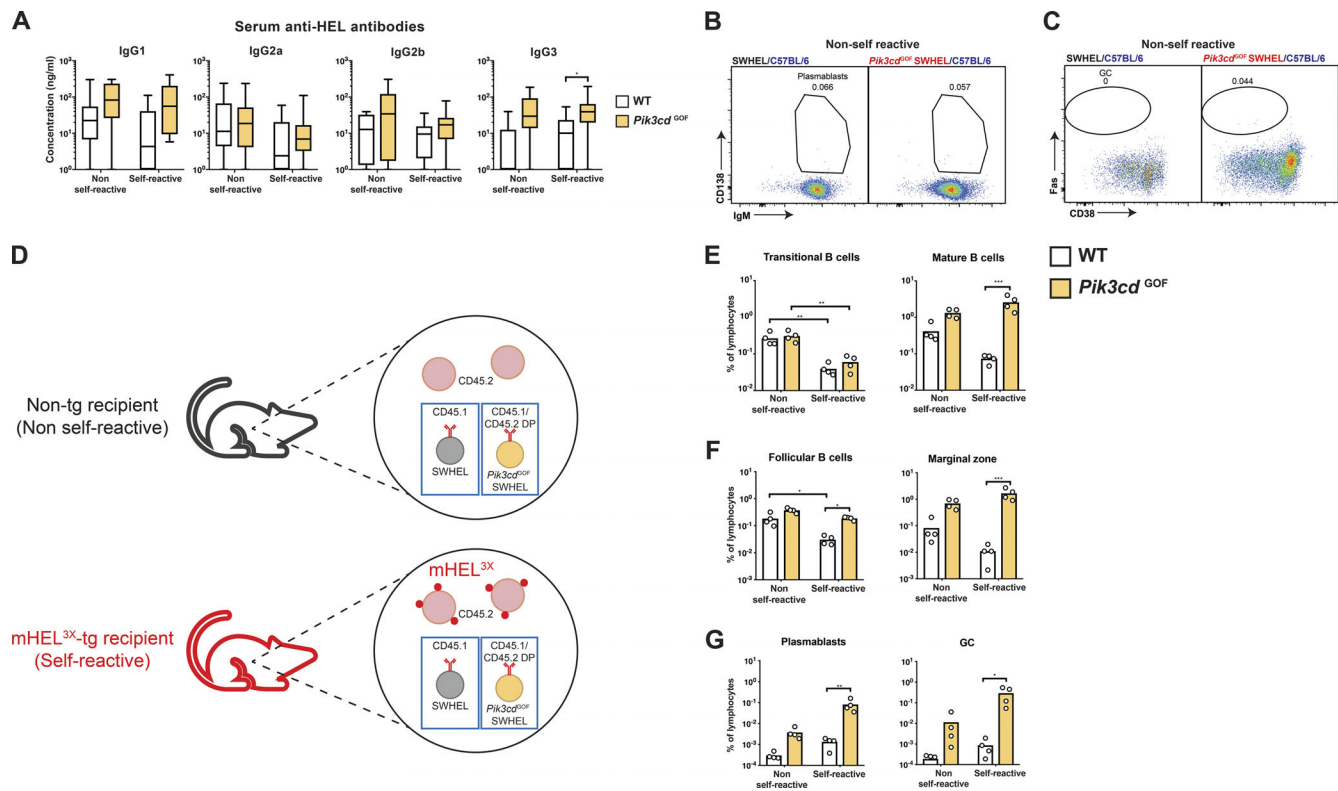
Figure S5. Serum Ig levels and GC and plasmablast formation in chimeric mice. (A) Serum levels of HEL-specific IgG1, IgG2a, IgG2b, and IgG3 in the indicated BM chimeric mice (the center line shows the median, box limits show the upper and lower quartiles, and whiskers show the minimum and maximum; $n = 15–20$ per group combined from nine different chimera harvests). **(B and C)** Plasmablasts (IgM+CD138hi; B) and GC B cells (CD38loFashi; C) were identified in spleens of non–self-reactive chimeras. **(D)** Mixed BM chimeras were prepared with a 40:40:20 mix of CD45.1+WT.SW$_{HEL}$Rag1−/−:CD45.1+CD45.2+ Pik3cd^{GOF}SW$_{HEL}$ Rag1−/−:CD45.2+ recipient-matched BM into WT (non–self-reactive) or HEL-3x transgenic (self-reactive) recipients. Spleens were harvested from mice 8–9 wk after reconstitution. **(E)** The numbers of transitional (CD93+) and mature (CD93−) HEL-binding B cells of each genotype were enumerated. **(F and G)** Numbers of mature follicular (CD23hiCD21lo) and MZ (CD21hiCD23lo) B cells (F) and plasmablasts (IgM+CD138hi) and GC (Fas+CD38−) B cells (G) were then determined. **(E–G)** Each point represents an individual mouse combined from two different chimera harvests, and bars show means. Significant differences were determined using two-way ANOVA. *, $P < 0.05$; **, $P < 0.01$; ***, $P < 0.001$.

Lau et al.
Activated PI3Kδ breaks B cell tolerance

Journal of Experimental Medicine
https://doi.org/10.1084/jem.20191336

S6